

70-18,896

NAGY, Mohamed El-Sayed, 1942-
SPATIALLY DEPENDENT STOCHASTIC BEHAVIOUR OF
COUPLED CORE REACTORS.

Iowa State University, Ph.D., 1970
Engineering, nuclear

University Microfilms, A XEROX Company, Ann Arbor, Michigan

SPATIALLY DEPENDENT STOCHASTIC BEHAVIOUR OF
COUPLED CORE REACTORS

by

Mohamed El-Sayed Nagy

A Dissertation Submitted to the
Graduate Faculty in Partial Fulfillment of
The Requirements for the Degree of
DOCTOR OF PHILOSOPHY

Major Subject: Nuclear Engineering

Approved:

Signature was redacted for privacy.

In Charge of Major Work

Signature was redacted for privacy.

Head of Major Department

Signature was redacted for privacy.

Dean of Graduate College

Iowa State University
Ames, Iowa

1970

TABLE OF CONTENTS

	Page
I. INTRODUCTION	1
II. LITERATURE SURVEY	9
III. REACTOR MODELS INVESTIGATED	17
IV. SPACE DEPENDENT NOISE THEORY	27
V. APPLICATION OF NOISE MODEL AND RESULTS	44
VI. CONCLUSIONS	93
VII. SUGGESTIONS FOR FURTHER WORK	95
VIII. LITERATURE CITED	96
IX. ACKNOWLEDGMENTS	100
X. APPENDIX	101

I. INTRODUCTION

This thesis is concerned with the analysis and description of the response of coupled core nuclear reactors, treated as linear systems, to driving functions which are not specific functions of time. The time dependence is known only in a statistical sense.

Analyses of such functions are based on the theory of random or stochastic processes.

A function $x(t)$ is said to be a random or stochastic function if the value of x at time t is predictable only in a statistical sense. In general the statistical properties are not independent of time and analyses must be carried out on an ensemble of random functions. An ensemble is a collection of noise records all having the same statistical properties.

For example, if the output from an ion chamber in a nuclear reactor were recorded for a period of time each day under identical conditions, each day's record would be a random function and the collection of records would constitute an ensemble. One might also think of performing the same experiment simultaneously on many identical reactors (if such could be obtained) to generate the ensemble of random functions.

It is obvious that a description of such a non-time

stationary process would be quite complex. Considerable simplification of the analysis results if the statistical properties are independent of time - such a system is said to be time stationary.

The analysis can be further simplified by introducing the ergodic hypothesis. An ergodic random process is a time stationary process that can be analyzed, from the statistical standpoint, by time-wise sampling one of the representative records of the ensemble. The ergodic assumption is often made as a matter of convenience but it is very difficult to justify it formally. The ergodic assumption allows one to work with a single time record so it is obvious that a considerable savings results. Developments of the noise theory in this thesis follow the ergodic assumption unless otherwise stated.

The auto correlation function (1) , $\Phi(\tau)$, of a time stationary random function, $x(t)$, is defined as

$$\Phi(\tau) = \overline{x(t) x(t+\tau)} \quad (1.1)$$

where the overbar designates the average value. There is a variable time displacement and for a time stationary process $\Phi(\tau)$ cannot be a function of time. If the averaging is done in an ensemble sense

$$\Phi(\tau) = \lim_{n \rightarrow \infty} \frac{1}{n} \sum_{i=1}^n x_i(t) x_i(t+\tau) \quad (1.2)$$

If the ergodic assumption is made, the averaging can be made time wise and the auto-correlation function becomes

$$\Phi(\tau) = \lim_{T \rightarrow \infty} \frac{1}{T} \int_{-\frac{T}{2}}^{\frac{T}{2}} x(t) x(t+\tau) dt . \quad (1.3)$$

The auto correlation function is said to be a description of the random function in the time domain, that is, it is a measure of how the function changes with time. However, the systems engineer is usually more accustomed to working in the frequency domain where the transfer function is the basic description of the system. In the application of noise analysis to nuclear reactors, a major portion of the reported research has been carried out in terms of the frequency spectrum of the random function.

Analysis in the frequency domain is based on the cross and power spectral densities. The power spectral density $\Phi_{ff}(\omega)$ of a function $f(t)$ is defined as

$$\Phi_{ff}(\omega) = \lim_{T \rightarrow \infty} \frac{1}{T} |F(\omega)|^2 \quad (1.4)$$

where $F(\omega)$ is the Fourier transform of the function $x(t)$ defined as

$$x(t) = \begin{cases} f(t) & |t| < \frac{T}{2} \\ 0 & |t| > \frac{T}{2} \end{cases} . \quad (1.5)$$

We note that as T becomes large more of the random function

is included in $x(t)$. It is a well known mathematical relationship (1) that the power spectral density and the autocorrelation function form a Fourier transform pair, thus

$$\Phi_{ff}(\omega) = \int_{-\infty}^{\infty} \Phi(\tau) e^{-j\omega\tau} d\tau \quad (1.6)$$

and

$$\Phi_{ff}(\tau) = \frac{1}{2\pi} \int_{-\infty}^{\infty} \Phi(\omega) e^{j\omega\tau} d\omega. \quad (1.7)$$

If one considers two random functions $x(t)$ and $y(t)$, the cross-correlation functions (4) associated with these functions are

$$\Phi_{xy}(\tau) = \lim_{T \rightarrow \infty} \frac{1}{T} \int_{-\frac{T}{2}}^{\frac{T}{2}} x(t) y(t+\tau) dt \quad (1.8)$$

or

$$\Phi_{yx}(\tau) = \lim_{T \rightarrow \infty} \frac{1}{T} \int_{-\frac{T}{2}}^{\frac{T}{2}} y(t) x(t+\tau) dt. \quad (1.9)$$

From these two formulas one can distinguish which function is shifted in time and the corresponding cross-correlation. As in the case of auto-correlation, the cross-correlation function is characterized in the frequency domain by its cross-spectral density function and they form Fourier transform pair as follows

$$\Phi_{xy}(\omega) = \int_{-\infty}^{\infty} \Phi_{xy}(\tau) e^{-j\omega\tau} d\tau \quad (1.10)$$

or

$$\Phi_{yx}(\omega) = \int_{-\infty}^{\infty} \Phi_{yx}(\tau) e^{-j\omega\tau} d\tau \quad (1.11)$$

and

$$\Phi_{xy}(\tau) = \frac{1}{2\pi} \int_{-\infty}^{\infty} \Phi_{xy}(\omega) e^{j\omega\tau} d\omega \quad (1.12)$$

$$\Phi_{yx}(\tau) = \frac{1}{2\pi} \int_{-\infty}^{\infty} \Phi_{yx}(\omega) e^{j\omega\tau} d\omega . \quad (1.13)$$

Cross and auto-correlation techniques have been used for discussing reactors transfer functions (25).

The relationships between the input and output of a system in terms of the transfer function and the power and cross-spectral densities are

$$\Phi_{ff}(\omega) = |KG(j\omega)|^2 \Phi_{xx}(\omega) \quad (1.14)$$

and

$$\Phi_{xf}(\omega) = KG(j\omega) \Phi_{xx}(\omega) \quad (1.15)$$

where

$\Phi_{ff}(\omega)$ = power spectral density of the output

$\Phi_{xx}(\omega)$ = power spectral density of the input

$\Phi_{xf}(\omega)$ = cross-spectral density between the input and output

$|KG(j\omega)|$ = magnitude of the system transfer function $KG(j\omega)$.

Another important function in noise analysis is the coherence function (27) which is defined as

$$R(\omega) = \frac{\Phi_{xf}(\omega)}{(\Phi_{xx}(\omega) \Phi_{ff}(\omega))^{1/2}} \quad (1.16)$$

Cross-correlation techniques have proven to be useful for studying nuclear reactor systems. Relationships between various system variables such as inlet and outlet core temperature, coolant flow rate, system pressure, and space dependent neutron flux variations have been investigated using these methods. The results of such measurements can be used to provide a more detailed understanding of the rather complex interactions taking place in the reactor.

The purpose of this thesis is to study the behavior of the space-dependent spectral density functions of the neutron level fluctuations for the thermal group flux of a two-energy group approximation. The input function is assumed to be white noise (20) caused by volume distributed fission sources. The term white noise is used as an analogy to white light which contains all frequency components over the visible spectrum and thus has a flat frequency distribu-

tion. In many applications a band limited random function may be assumed to approximate white noise if the spectrum is flat over the range of frequencies that are important in the analysis.

The study is to be carried out for a one dimensional model of the Iowa State University UTR-10 coupled core Argonaut type reactor (18). The UTR-10 reactor is a water moderated and graphite reflected system licensed for operation up to 10 kw. The effect of changing the thickness and material of the coupling region (internal reflector) on the behavior of the spatially-dependent spectral-density functions and the corresponding coherence function (3) is to be studied. Neutron detector spacing will be used as a parameter. Graphite, heavy water and beryllium are the three materials to be considered as internal reflectors. Effect of removal and absorption cross-sections of the coupling regions on the behavior of spectral densities will also be considered.

In view of the increased consideration being given to coupled fast-thermal power reactors, large thermal reactors which can show coupling properties for regions far from each other and the clustering of nuclear rockets a better understanding of coupling effects is desirable.

The specific goal of this study is to determine which parameters in the coupling region have an important

effect on the spatially-dependent noise response of a family of coupled core reactors based upon a UTR-10 prototype model.

II. LITERATURE SURVEY

In noise analysis one should distinguish between analysis based on point reactor kinetics, nodal analysis (3, 27, 2) in which a reactor is represented by finite number of points and modal analysis (21, 29, 30, 8) in which a reactor is represented as a continuous system.

The only published work which includes spatially-dependent noise analysis for coupled core reactors is that by Danofsky (8), Hendrickson (13), and Seifritz and Albrecht (27). Danofsky calculated the space-dependent cross-spectral-density function for the Iowa State University UTR-10 Reactor, a commercial version of the coupled-core Argonaut reactor (18). Hendrickson (13) measured the cross-spectral density experimentally for the Iowa State University UTR-10 Reactor and he was the first to detect the existence of the sink (zero) frequency of this function. Seifritz and Albrecht (27) measured the coherence function in an Argonaut reactor with both a ring core loading and a two slab loading.

An analysis of the spatially dependent response of a reactor to an oscillating absorber was first attempted by Weinberg and Schweinler (31) in 1948. Since that time almost all efforts aimed at describing the spatial dependence of the reactor response have been based on modal expansion techniques in which the space and time-dependent flux, $\phi(x,t)$, is approximated by a series of products of space

modes, $\psi_i(x)$, and time dependent coefficients, $a_i(t)$. The flux is approximated by

$$\phi(x,t) = \sum_{i=1}^N a_i(t) \psi_i(x) .$$

In this type of analysis, there are two steps, the selection of the space modes and the determination of the time coefficients.

Several methods have been suggested for obtaining the space modes. Foderaro and Garabedian (10, 11) used functions which are solution of the Helmholtz equation

$$\nabla^2 \psi + \beta^2 \psi = 0$$

to study the response of a reactor having an internal reflector. The difficulty in using those modes arise from the fact that one requires many terms in the expansion for complex geometries. Modes which are also eigen functions are the lambda and omega modes (14, 15). The lambda modes are obtained by solving an eigenvalue problem of the form

$$L\psi_n = \frac{1}{\lambda_n} M\psi_n$$

where the L-operator is the multigroup removal operator and the M-operator is the multigroup production operator.

The omega modes are obtained by solving an expansion of the form

$$[L-M]\psi_n = \omega_n T\psi_n$$

where T is the diagonal matrix whose elements are the reciprocal neutron group speeds. Kaplan (15) and Gyftopoulos (12) have used the natural mode approximation to obtain the space modes and time coefficients by solving an equation of the form

$$L_0\psi_n = \omega_n\psi_n$$

where the L_0 -operator is the steady-state operator which results when the multigroup equations are put into the form

$$L\phi = \dot{\phi}$$

where

$$\phi = \text{Col}[\phi_F \phi_S C]$$

and

$$L_0\phi_0 = 0.$$

The fast flux, slow flux and precursor concentration are represented by ϕ_F , ϕ_S and C respectively.

Dougherty and Shen (9) propose the use of Green's function modes, which are nonorthogonal modes and are obtained by solving the diffusion equation with sources fixed in various subregions of the reactor. To obtain these modes one divides the reactor into regions equal to the number of modes desired for the analysis. A distributed source is

introduced into each region by using a fission source in multiplying regions and a pseudo source into nonmultiplying regions. It has been shown that the solution to problems involving localized step change in reactivity (6) converges much faster for Green's modes than for Helmholtz modes.

In space-dependent reactor noise analysis, different techniques have been used for describing the stochastic component of the neutron flux. Moore (21) studied the space dependence of the neutron noise field of a reactor using double series expansions of eigenfunctions of the Helmholtz equation to express the source-correlation field and the auto- and cross-correlation noise. He used the orthogonality of the space eigenfunction to derive the differential equation for the time coefficients. Moore (21) applied his study to a one energy group bare model. Sheff and Albrecht (29, 30) developed a space-dependent stochastic fluctuation theory using Langevin's technique for finding the appropriate Green's function for the mean-neutron-density equation of the system in question. The technique, they used, yields the cross correlation function as a double convolution over two Green's functions. They used one-energy-group diffusion theory for solving an unreflected homogeneous cubical reactor.

Osborn and Natelson (24) derived a space-dependent kinetic equation for neutrons from a quantum Liouville equation. Their analysis was reduced to one energy group and

ignoring delayed neutron effect.

Natelson, Osborn and Shure (22) applied the space and energy analysis, that was developed by Osborn and Natelson (24), to analyze power spectral density experiment (26) using two group diffusion approximation for a homogenous bare reactor. Akcasu and Osborn (1) developed the space-and energy-dependent theory of reactor-noise analysis using Langevin's technique starting from the transport equations. Their general theory was applied to bare reactor models considering one speed diffusion approximation. They established a connection between Langevin's technique and the doublet theory based on the Liouville equation (24) and showed that the two techniques give identical results.

In this thesis, the stochastic component of the neutron flux is described by an expansion in Green's modes (16). This leads to correlation functions which are double series expansions of space modes and correlation functions of the time dependent coefficients. The analysis is based on Danofsky's development (8) of a space-dependent noise formulation.

Danofsky (8) explained the advantage of using Green's modes in approximating the flux and he showed a comparison between the Green's modes and the natural mode approximation (5) for obtaining the space-dependent frequency response. Green's modes were used by Carter (6) as the space functions

for solving the space-time kinetic equations for coupled-core reactors. Merritt (19) used Green's modes for obtaining the spatially dependent frequency response of coupled core reactors and he analyzed a family of coupled cores nuclear reactors based upon a UTR-10 prototype model.

In this work five Green's modes, $\psi_i(x)$, are used to approximate the steady state flux, $\phi(x,0)$. The time dependent flux, $\phi(x,t)$ is approximated by a series of products of the modes, $\psi_i(x)$, and time-dependent coefficients $a_i(t)$. The flux is approximated by

$$\phi(x,t) \equiv \sum_{i=1}^5 a_i(t) \psi_i(x)$$

which converges to the steady state flux, $\phi(x,0)$, by setting all the time coefficients, $a_i(t)$, equal to unity, thus

$$\phi(x,0) = \sum_{i=1}^5 \psi_i(x) \quad .$$

Since the forcing function of the system is white noise one expects the time coefficients, $a_i(t)$, to be stochastic in nature.

The stochastic coherence function as examined by Albrecht and Seifritz (27) for two node nuclear reactor model was given as the ratio of the cross-spectral density function between two random signals $n_1(t)$ and $n_2(t)$, $\phi_{n_1 n_2}(\omega)$ and the square root of the product of the respective auto spectral densities $\phi_{n_1 n_1}(\omega)$ and $\phi_{n_2 n_2}(\omega)$. Thus the

coherence function, $R(\omega)$, can be written as

$$R(\omega) = \frac{\Phi_{n_1 n_2}(\omega)}{(\Phi_{n_1 n_1}(\omega) \Phi_{n_2 n_2}(\omega))^{1/2}}$$

It was pointed out in (3) that for coupled systems it is much better to discuss the properties of the coherence function than those of the cross spectral density function since the coherence function depends only on the coupling between the regions being sampled by the detectors whereas the cross spectral density function depends on the individual characteristics of the region. Thus coupling parameters alone enter the coherence function while the cross spectrum is more complicated. An illustration of this point is the coherence function for a one point reactor model which is unity, representing complete coupling between detector signals, and the cross spectrum yields dynamic information. The importance of the coherence function in general for coupled core systems comes from the fact that one can measure the subcriticality of a single node and the mean time delay associated with the coupling between nodes (27).

A special value of using the coherence function is that coupling characteristics normally measured by transient methods can also be measured in a steady-state reactor without an external perturbation. For a two node, symmetrical core (27) the mean time delay is found by identifying the

frequency at which the coherence function passes through zero, (the sink frequency (13)), and the nodal reactivity is determined from the characteristic break frequency of the coherence function.

In this thesis a space-dependent continuous model is used. One can obtain the two node symmetric analysis as a special case, if cross correlation between the center of the two cores is performed. As stated by Seifritz, Stegemann and V  th (28), a zero-power noise analysis is interesting for the study of fast-thermal coupled systems as well as for the determination of reactivity values and absolute reactor power.

III. REACTOR MODELS INVESTIGATED

The prototype reactor to be studied is a one-dimensional model of the Iowa State University UTR-10 reactor which is shown in Figure 3.1. To show the effect of coupling region thickness on the cross-spectral density, a family of reactors based upon a UTR-10 prototype model with different thicknesses of the coupling region was investigated. All the systems under investigation are delayed critical. The two-energy-group nuclear data, which represent the original delayed

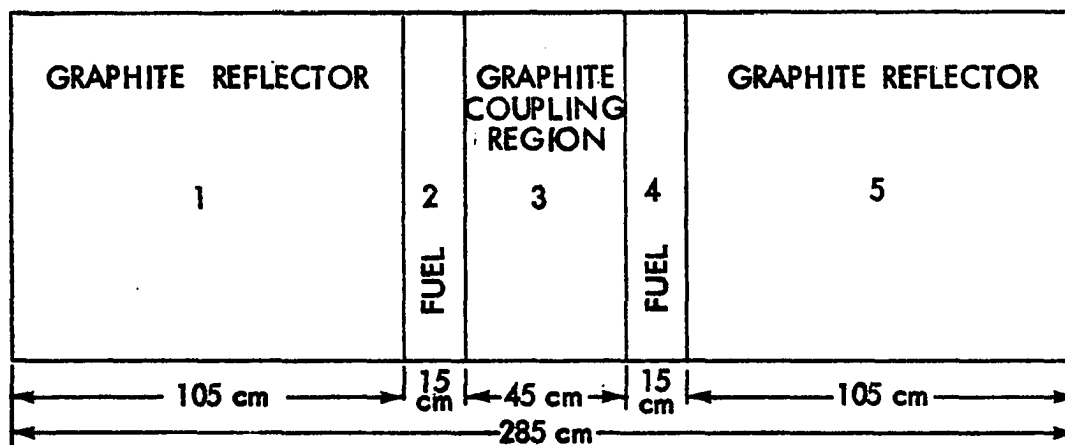


Figure 3.1. UTR-10 Reactor model

critical reactor, are shown in Table 3.1. In this diffusion theory approximation, absorption in the fast group and fast fission were considered to be negligible and photoneutrons also were neglected when heavy water and beryllium were used. It was assumed that the U-235 content was the same in each

core tank and unless otherwise stated this will also be the case in all the other modified systems.

In all the modified systems as well as in the original reactor models the leakage of neutrons through the two sides and top and bottom of the reactor are described by the transverse buckling. This was obtained by making a horizontal and vertical flux map through a core tank, extrapolating the fluxes to zero and obtaining the buckling, B_z , in each direction by assuming the flux obeyed an equation of the form

$$\phi(z) = A \sin B_z z .$$

The total transverse buckling, B_T^2 , is the sum of the two components

$$B_T^2 = B_y^2 + B_z^2 = 0.00216 \text{ cm}^{-2} .$$

In addition to changing the coupling region size, the coupling region material was varied. The other materials that were used are heavy water and beryllium.

All the modified reactors have the same parameters as in Table 3.1 with the exception of the coupling region size, coupling region material and its nuclear parameters.

The thermal absorption cross-section of a uniformly distributed control poison in the fuel was adjusted to keep the reactor critical. Symmetric adjustments were made to avoid generating flux tilt in the reactor.

Table 3.1. Prototype reactor critical parameters

Reactor parameter	Region 1	Region 2	Region 3	Region 4	Region 5
$\Sigma_R \text{ cm}^{-1}$	0.00276	0.0267	0.00276	0.0267	0.00276
$\Sigma_a \text{ cm}^{-1}$	0.00024	0.09079	0.00024	0.09079	0.00024
$D_F \text{ cm}$	1.016	1.23	1.016	1.23	1.016
$D_S \text{ cm}$	0.84	0.1894	0.84	0.1894	0.84
$\nu \Sigma_F \text{ cm}^{-1}$	0	0.122	0	0.122	0
$R_S \text{ cm}$	105	15	45	15	105
$v_F \text{ cm/sec}$	4.36×10^8				
$v_T \text{ cm/sec}$	2.2×10^5				
$\lambda \text{ sec}^{-1}$	0.08				
β	0.0064				
Σ_R = fast removal cross section			v_F = fast velocity		
Σ_a = thermal absorption cross section			v_T = thermal velocity		
D_F = fast diffusion coefficient			λ = precursor decay constant		
D_S = slow diffusion coefficient			β = delayed neutron fraction		
Σ_f = fission cross section					
ν = average number of neutrons per fission					
R_S = region size					

The critical thermal absorption cross section of the two fuel regions was determined by the usual technique of solving the criticality determinant for the two-group diffusion equation. Fluxes and adjoint fluxes were assumed to go to zero at the extrapolated boundaries of the reactor,

$$\phi(0) = \phi(T) = 0 \quad \text{and} \quad \phi^*(0) = \phi^*(T) = 0 \quad . \quad (3.1)$$

The fluxes and their currents were assumed to be continuous at all internal material interfaces,

$$\phi(x_j^-) = \phi(x_j^+) \quad , \quad \phi^*(x_j^-) = \phi^*(x_j^+) \quad (3.2)$$

also

$$D_j \frac{d\phi}{dx} \Big|_{x_j^-} = D_{j+1} \frac{d\phi}{dx} \Big|_{x_j^+} \quad \text{and} \quad D_j \frac{d\phi^*}{dx} \Big|_{x_j^-} = D_{j+1} \frac{d\phi^*}{dx} \Big|_{x_j^+} \quad . \quad (3.3)$$

Where

$$\phi = \text{Col}[\phi_F \ \phi_S], \quad \phi^* = \text{Col}[\phi_F^* \ \phi_S^*] \quad \text{and} \quad D_j = \begin{bmatrix} D_{Fj} \\ \\ \\ D_{Sj} \end{bmatrix} \quad . \quad (3.4)$$

The x_j corresponds to the reactor material interfaces and T is equal to the reactor thickness. Also the fluxes $\phi(x)$ and the adjoints $\phi^*(x)$ are finite and nonnegative.

Applying the above conditions, 3.1, 3.2 and 3.3, to the two-group diffusion equations a $2m \times 2m$ set of homogeneous equations results

$$\underline{AC} = 0 \quad (3.5)$$

where m is two times the number of internal material interfaces plus two. The reactor is adjusted to criticality by changing the thermal absorption cross section, in the fuel region, so that the determinant of the coefficient matrix, A , is zero. Following this technique the critical parameters for different sizes and materials of the coupling regions were obtained as shown in Tables 3.2 and 3.3.

The effect of the removal cross section on the spectral-density function was demonstrated by modifying the removal cross section of heavy water keeping other parameter constant. Also, the absorption cross section of heavy water was modified keeping other parameters constant as shown in Table 3.5.

Table 3.2. Fuel region critical absorption cross section for graphite coupling region

Coupling region size cm	Critical absorption cross section cm^{-1}	Coupling region size cm	Critical absorption cross section cm^{-1}	Coupling region size cm	Critical absorption cross sec- tion cm^{-1}
25	0.09351	45	0.09079	85	0.08912
35	0.09190	55	0.09006		
40	0.09129	75	0.08930		

Table 3.3. Fuel region critical absorption cross section for heavy water coupling region

Coupling region size cm	Critical absorption cross section cm^{-1}	Coupling region size cm	Critical absorption cross section cm^{-1}	Coupling region size cm	Critical absorption cross section cm^{-1}
20	0.09492	40	0.09103	65	0.08892
25	0.09373	45	0.09041	75	0.08854
35	0.09178	55	0.08955		

The two group nuclear constants of graphite, heavy water and beryllium were obtained from Lamarsh (17). For heavy water and beryllium those constants are shown in Table 3.4.

Table 3.4. Nuclear constants for heavy water and beryllium

Material	D_F cm	D_S cm	Σ_R cm^{-1}	Σ_a cm^{-1}
heavy water	1.29	0.87	0.00985	0.000029
beryllium	0.562	0.50	0.00551	0.00104

Beryllium as a coupling material was investigated for the 45 cm case only. The corresponding critical absorption cross section was found to be 0.09311 cm^{-1} .

Since the set of parameters which makes the reactors critical is now specified, the solution of the two-group diffusion equations may be evaluated in each region of the reactor after solving for the matrix of coefficients, \underline{A} , in

Equation (3.5). From this solution the fast- and thermal-group fluxes can be calculated. A similar procedure is followed for the adjoint system.

Table 3.5. Critical parameters for a 45 cm modified heavy water coupling region

$\Sigma_R \text{ cm}^{-1}$	$\Sigma_a \text{ cm}^{-1}$	Critical absorption cross section cm^{-1}
0.00985	0.000029	0.09041
0.00985	0.00024	0.08994
0.00985	0.00199	0.08727
0.00551	0.000029	0.08999
0.00276	0.000029	0.08962

Typical neutron flux distributions for reactors with 45 cm coupling regions of graphite, heavy water and beryllium are shown in Figures 3.2 and 3.3.

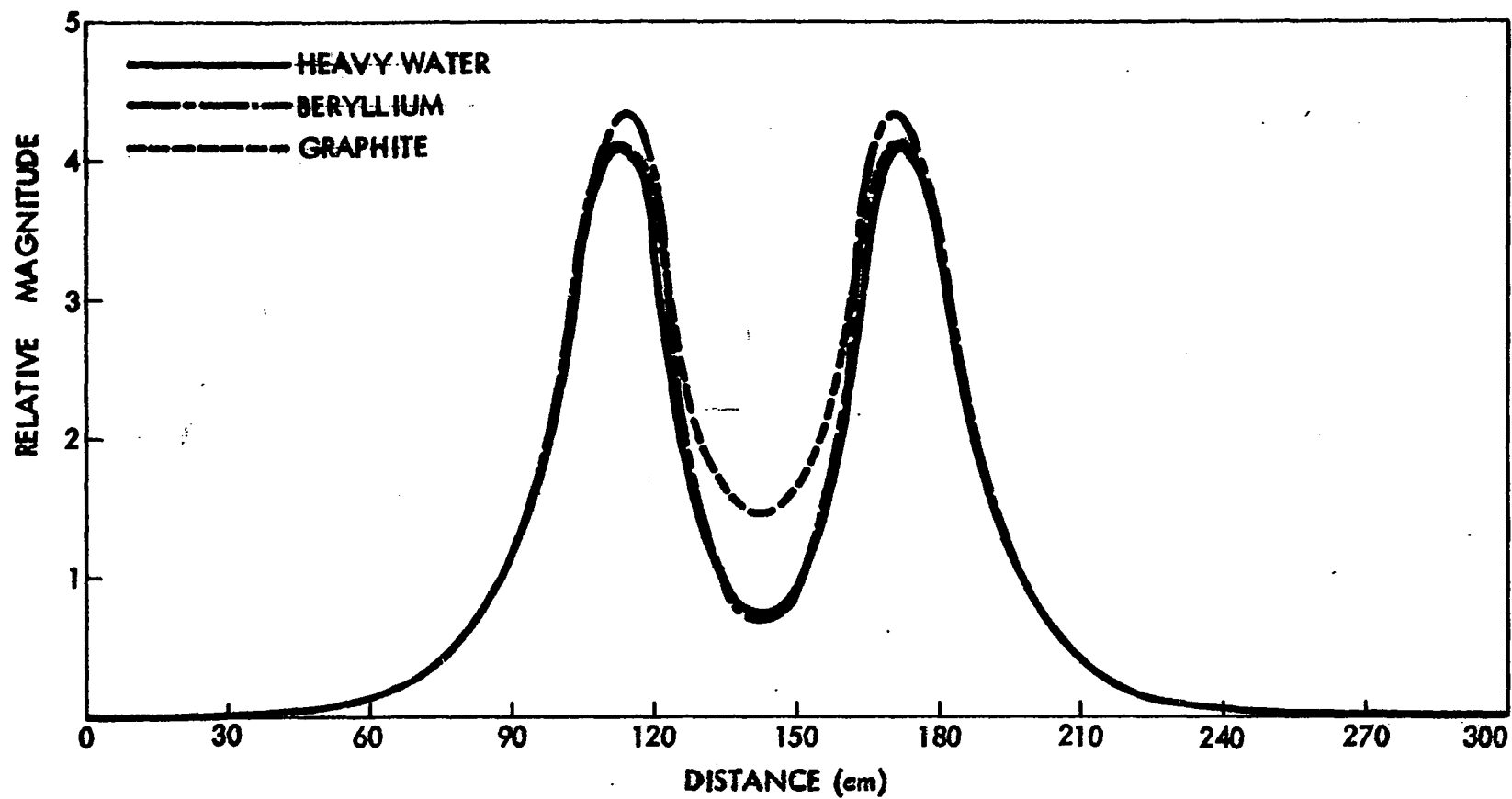


Figure 3.2. Fast flux distribution for three different 45 cm coupling region material

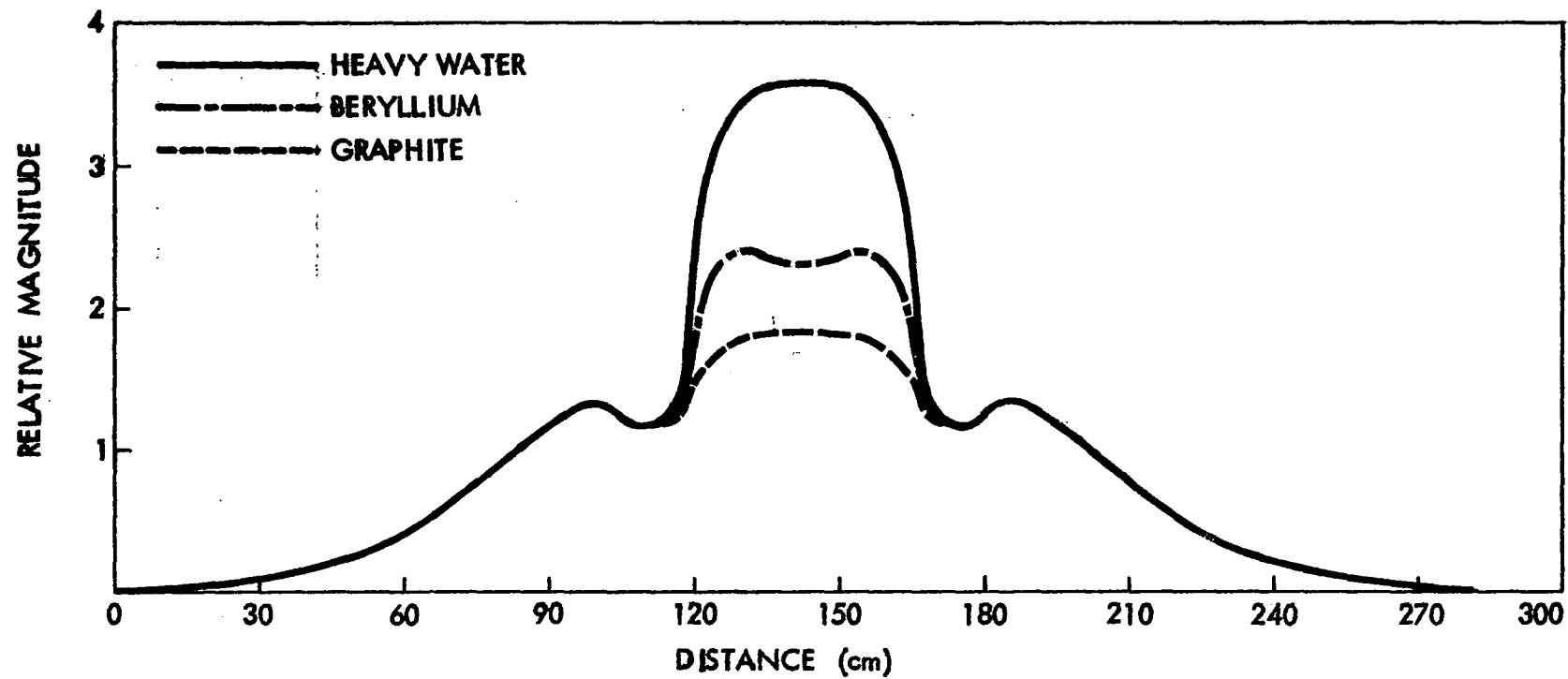


Figure 3.3. Slow flux distribution for three different coupling region materials with 45 cm thickness

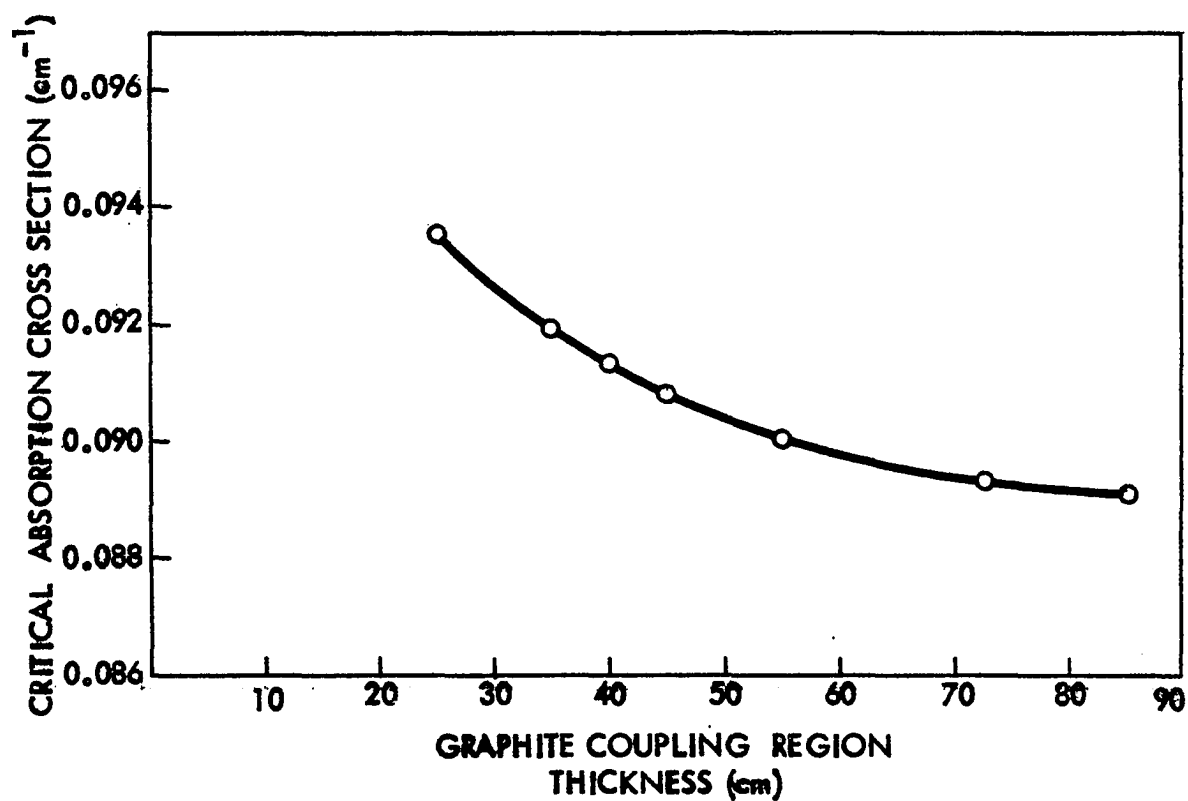


Figure 3.4. Critical absorption cross section as a function of graphite coupling region thickness

IV. SPACE DEPENDENT NOISE THEORY

In this section the formal development of the space dependent noise theory based on an analysis technique described by Danofsky (8) is presented.

Consider the M^{th} order modal analysis expression for the flux

$$\phi(x,t) = \sum_{i=1}^M A_i(t) \psi_i(x) . \quad (4.1)$$

Where $A_i(t)$ are time dependent expansion coefficients and $\psi_i(x)$ are the space modes.

In this development it is convenient to consider $\phi(x,t)$ as one of the group fluxes of a multigroup diffusion theory approximation.

Equation (4.1) can be expressed as the sum of steady state plus a small time dependent component as follows

$$\begin{aligned} \phi(x,t) &= \phi_0(x) + \Delta\phi(x,t) \\ &= \sum_{i=1}^M \psi_i(x) + \sum_{i=1}^M \Delta A_i(t) \psi_i(x) . \end{aligned} \quad (4.2)$$

For our analysis, $\Delta\phi(x,t)$ represents the variation in the neutron flux due to ergodic stochastic driving functions which are not defined yet, and the $\Delta A_i(t)$ are stochastic expansion coefficients. We will assume that the time dependent component that we will use has zero average value.

One can form the auto- or cross-correlation function for the variation of the flux as follows

$$\begin{aligned}\Phi(x_\rho, x_k, \tau) &= \overline{\Delta\phi(x_\rho, t) \Delta\phi(x_k, t+\tau)} \\ &= \sum_{i=1}^M \overline{\Delta A_i(t) \psi_i(x_\rho)} \times \sum_{j=1}^M \overline{\Delta A_j(t+\tau) \psi_j(x_k)}\end{aligned}\quad (4.3)$$

Where the overbar shows that a time average value of the product with the variable time delay τ is to be taken and $\Phi(x_\rho, x_k, \tau)$ gives the cross correlation function between two space points ρ and k if $\rho \neq k$ and the auto correlation function if $\rho = k$, however if $\rho = k$ and $\Delta\phi(x_\rho, t)$ is not of the same energy group as $\Delta\phi(x_k, t+\tau)$ a cross correlation between energy group results. A cross correlation between space points and energy groups could be developed if $\rho \neq k$ and $\Delta\phi(x_\rho, t)$ is not of the same energy group as $\Delta\phi(x_k, t+\tau)$.

Equation (4.3) is expanded to give

$$\begin{aligned}\Delta\phi(x_\rho, t) \times \Delta\phi(x_k, t+\tau) &= [\Delta A_1(t) \psi_1(x_\rho) + \Delta A_2(t) \psi_2(x_\rho) \\ &\quad + \dots + \Delta A_M(t) \psi_M(x_\rho)] \\ &\quad \times [\Delta A_1(t+\tau) \psi_1(x_k) + \Delta A_2(t+\tau) \psi_2(x_k) \\ &\quad + \dots + \Delta A_M(t+\tau) \psi_M(x_k)] .\end{aligned}$$

which upon expanding yields

$$\begin{aligned}
 & \Delta A_1(t) \Delta A_1(t+\tau) \psi_1(x_\rho) \psi_1(x_k) + \Delta A_1(t) \Delta A_2(t+\tau) \psi_1(x_\rho) \psi_2(x_k) \\
 & + \dots + \Delta A_1(t) \Delta A_M(t+\tau) \psi_1(x_\rho) \psi_M(x_k) \\
 & + \dots + \Delta A_M(t) \Delta A_1(t+\tau) \psi_M(x_\rho) \psi_1(x_k) \\
 & + \dots + \Delta A_M(t) \Delta A_M(t+\tau) \psi_M(x_\rho) \psi_M(x_k) . \quad (4.4)
 \end{aligned}$$

Equation (4.4) may be written as

$$\Delta \phi(x_\rho, t) \Delta \phi(x_k, t+\tau) = \sum_{i=1}^M \sum_{j=1}^M \Delta A_i(t) \Delta A_j(t+\tau) \psi_i(x_\rho) \psi_j(x_k) . \quad (4.5)$$

Time averaging yields

$$\begin{aligned}
 \Phi(x_\rho, x_k, \tau) &= \overline{\Delta \phi(x_\rho, t) \Delta \phi(x_k, t+\tau)} \\
 &= \sum_i \sum_j \Gamma_{ij}(\tau) \psi_i(x_\rho) \psi_j(x_k) \quad (4.6)
 \end{aligned}$$

where

$$\Gamma_{ij}(\tau) = \overline{\Delta A_i(t) \Delta A_j(t+\tau)} .$$

One should note that $\Gamma_{ij}(\tau)$ is a correlation function of the time coefficients. Equation (4.6) represents the space-dependent cross- or auto-correlation function of the neutron-level variations in the reactor where the form of $\Gamma_{ij}(\tau)$ depends on the properties of the forcing function.

To obtain the frequency domain equivalent of Equation (6) Fourier transform both sides of the equation to obtain

$$\Phi(x_\rho, x_k, \omega) = \sum_{ij} \Gamma(\omega) \psi_i(x_\rho) \psi_j(x_k) \quad (4.7)$$

where

$$\Gamma_{ij}(\omega) = \int_{-\infty}^{\infty} \Gamma_{ij}(\tau) \exp(-j\omega\tau) d\tau$$

and

$$\Phi(x_\rho, x_k, \omega) = \int_{-\infty}^{\infty} \Phi(x_\rho, x_k, \tau) \exp(-j\omega\tau) d\tau .$$

Thus the problem of obtaining the space-dependent auto- or cross-spectral density requires knowledge of the auto- or cross-spectral densities between the time coefficients. These are easy to obtain for some modal-expansion techniques. The formulation that will be derived here is quite general and may be used to calculate the correlation and spectral-density functions between any two members of the group fluxes or for any of the group fluxes for any combination of space points.

For most model-analysis methods the time coefficients are given by a set of differential equations (14, 8) of the form

$$\bar{D}\Delta\bar{A}(t) = \bar{F}(t) \quad (4.8)$$

Where \bar{D} is a matrix whose elements are constants and linear differential operators, $\Delta\bar{A}$ is a vector containing the

time coefficients and \bar{F} is a vector of driving functions.

A general form of Equation (4.8) can be shown as follows

$$\begin{aligned} D_{11}\Delta A_1(t) + D_{12}\Delta A_2(t) + \dots + D_{1n}\Delta A_n(t) &= f_1(t) \\ D_{21}\Delta A_1(t) + D_{22}\Delta A_2(t) + \dots + D_{2n}\Delta A_n(t) &= f_2(t) \\ D_{n1}\Delta A_1(t) + D_{n2}\Delta A_2(t) + \dots + D_{nn}\Delta A_n(t) &= f_n(t) \end{aligned} \quad (4.9)$$

Where D_{ij} are linear differential operators, ΔA_i are time coefficients and $f_j(t)$ are driving functions. It is assumed here that ΔA_i and $f_j(t)$ are time stationary ergodic functions. Introduce the output correlation function

$$\Gamma_{ij}(\xi) = \lim_{T \rightarrow \infty} \frac{1}{T} \int_{-\frac{T}{2}}^{\frac{T}{2}} \Delta A_i(t) \Delta A_j(t+\xi) dt \quad (4.10)$$

and input correlation functions

$$\begin{aligned} \chi_{pm}(\xi) &= \overline{f_p(t) f_m(t+\xi)} \\ &= \lim_{T \rightarrow \infty} \frac{1}{T} \int_{-\frac{T}{2}}^{\frac{T}{2}} f_p(t) f_m(t+\xi) dt \end{aligned} \quad (4.11)$$

Where Γ_{ij} and χ_{pm} are matrix elements of a general input correlation matrix Γ and a general output matrix χ . There are related spectral density matrices $\hat{\Gamma}$ and $\hat{\chi}$.

Now to develop the desired relationship operate on Equation (4.10) with \bar{D}_{pj} which is the same as D_{pj} except differentiation is taken with respect to ξ rather than t .

The result is

$$\bar{D}_{pj} \Gamma_{ij}(\xi) = \lim_{T \rightarrow \infty} \frac{1}{T} \int_{-\frac{T}{2}}^{\frac{T}{2}} \Delta A_i(t) \bar{D}_{pj} \Delta A_j(t+\xi) dt. \quad (4.12)$$

Add these up for all j to obtain

$$\sum_{j=1}^n \bar{D}_{pj} \Gamma_{ij}(\xi) = \lim_{T \rightarrow \infty} \frac{1}{T} \int_{-\frac{T}{2}}^{\frac{T}{2}} \Delta A_i(t) \left[\sum_{j=1}^n \bar{D}_{pj} \Delta A_j(t+\xi) \right] dt. \quad (4.13)$$

Note the derivatives with respect to ξ in \bar{D}_{pj} may be replaced with derivatives with respect to $(t+\xi)$ thus the sum on the right side of Equation (4.13) is the same as the p^{th} equation in (4.9) with t replaced with $t+\xi$. Here we have then

$$\sum_{j=1}^n \bar{D}_{pj} \Delta A_j(t+\xi) = f_p(t+\xi)$$

and Equation (4.13) becomes

$$\sum_{j=1}^n \bar{D}_{pj} \Gamma_{ij}(\xi) = \lim_{T \rightarrow \infty} \frac{1}{T} \int_{-\frac{T}{2}}^{\frac{T}{2}} \Delta A_i(t) f_p(t+\xi) dt. \quad (4.14)$$

Let $\gamma = t+\xi$ to obtain

$$\sum_{j=1}^n \bar{D}_{pj} \Gamma_{ij}(\xi) = \lim_{T \rightarrow \infty} \frac{1}{T} \int_{-\frac{T}{2}}^{\frac{T}{2}} f_p(\gamma) \Delta A_i(\gamma-\xi) d\gamma. \quad (4.15)$$

Since γ is a dummy of integration one can let $\gamma=t$ again to obtain

$$\sum_{j=1}^n \bar{D}_{pj} \Gamma_{ij}(\xi) = \lim_{T \rightarrow \infty} \frac{1}{T} \int_{-\frac{T}{2}}^{\frac{T}{2}} f_p(t) \Delta A_i(t-\xi) dt. \quad (4.16)$$

Next introduce the operators \bar{D}_{qi} which operate on ξ and have the signs changed on all derivatives of odd power.

Operation on Equation (4.16) yields

$$\sum_{j=1}^n \bar{D}_{qi} \bar{D}_{pj} \Gamma_{ij}(\xi) = \lim_{T \rightarrow \infty} \frac{1}{T} \int_{-\frac{T}{2}}^{\frac{T}{2}} f_p(t) \bar{D}_{qi} \Delta A_i(t-\xi) dt. \quad (4.17)$$

Summation on the i index gives

$$\sum_{i=1}^n \sum_{j=1}^n \bar{D}_{qi} \bar{D}_{pj} \Gamma_{ij}(\xi) = \lim_{T \rightarrow \infty} \frac{1}{T} \int_{-\frac{T}{2}}^{\frac{T}{2}} f_p(t) \left[\sum_{i=1}^n \bar{D}_{qi} \Delta A_i(t-\xi) \right] dt \quad (4.18)$$

one can show that differentiating \bar{D}_{qi} with respect to ξ is equal to \bar{D}_{qi} , differentiating with respect to $(t-\xi)$.

Thus the sum on the right side of Equation (4.18) is the same as the q^{th} equation in (4.9) with t replaced by $t-\xi$.

Thus we have

$$\sum_{i=1}^n \bar{D}_{qi} \Delta A_i(t-\xi) = f_q(t-\xi)$$

and Equation (4.18) becomes

$$\sum_{i=1}^n \sum_{j=1}^n \bar{D}_{qi} \bar{D}_{pj} \Gamma_{ij}(\xi) = \lim_{T \rightarrow \infty} \frac{1}{T} \int_{-\frac{T}{2}}^{\frac{T}{2}} f_p(t) f_q(t-\xi) dt. \quad (4.19)$$

Making the change in variable $M=t-\xi$ and replacing M by t again, since M is a dummy variable, one obtains

$$\sum_{i=1}^n \sum_{j=1}^n \bar{D}_{qi} \bar{D}_{pj} \Gamma_{ij}(\xi) = \lim_{T \rightarrow \infty} \frac{1}{T} \int_{-\frac{T}{2}}^{\frac{T}{2}} f_q(t) f_p(t+\xi) dt, \quad (4.20)$$

thus

$$\sum_{i=1}^n \sum_{j=1}^n \bar{D}_{qi} \bar{D}_{pj} \Gamma_{ij}(\xi) = \chi_{qp}(\xi) . \quad (4.21)$$

Equation (4.21) represents a system of n^2 linear differential equations in the $\Gamma_{ij}(\xi)$. This can be changed to a set of algebraic equations by Fourier transforming both sides of Equation (4.21). Thus

$$\sum_{i=1}^n \sum_{j=1}^n \hat{D}_{qi}^* \hat{D}_{pj} \hat{\Gamma}_{ij}(\omega) = \hat{\chi}_{qp}(\omega) \quad (4.22)$$

where \hat{D}_{qi}^* is the complex conjugate of \hat{D}_{qi} and is obtained from \bar{D}_{qi} by replacing $\frac{d}{d\xi}$ with j . Also \hat{D}_{qi} is obtained from \bar{D}_{qi} by replacing $\frac{d}{d\xi}$ with j .

Equation (4.22) can be written in the matrix form

$$\hat{D}^* \hat{\Gamma} \hat{D}^T = \hat{\chi} \quad (4.23)$$

and

$$\hat{\Gamma} = (\hat{D}^*)^{-1} \hat{\chi} (\hat{D}^T)^{-1} \quad (4.24)$$

where

$$\hat{\Gamma} = \begin{bmatrix} \hat{\Gamma}_{11} & \hat{\Gamma}_{12} & \dots & \hat{\Gamma}_{1n} \\ \vdots & & & \\ \hat{\Gamma}_{n1} & \hat{\Gamma}_{n2} & \dots & \hat{\Gamma}_{nn} \end{bmatrix} \quad (4.25)$$

$$\hat{\chi} = \begin{bmatrix} \hat{\chi}_{11} & \hat{\chi}_{12} & \cdots & \hat{\chi}_{1n} \\ \hat{\chi}_{n1} & \hat{\chi}_{n2} & \cdots & \hat{\chi}_{nn} \end{bmatrix} \quad (4.26)$$

The elements, $\hat{\chi}_{qp}$, of the $\hat{\chi}$ matrix depend on the driving functions, $f(t)$, since

$$\hat{\chi}_{qp} = \int_{-\infty}^{\infty} \lim_{T \rightarrow \infty} \int_{-\frac{T}{2}}^{\frac{T}{2}} f_q(t) f_p(t+\xi) \exp(-j\omega\xi) dt d\xi .$$

Proper choice of the elements of $f(t)$ can simulate volume distributed or totalized production or destruction sources having arbitrary frequency spectra.

Using semidirect variational method (9), the time dependent coefficients of the modal expansion of the neutron fluxes are given by the Euler-Lagrange equations obtained from a variational principle for the multigroup kinetic equations. For this analysis Euler-Lagrange equations can be written in matrix form

$$\Lambda A = K A \quad (4.27)$$

where for an M^{th} -order two-energy-group expansion, A is a vector with $2M$ elements. In this analysis $M=5$. The first M elements are the expansion coefficients for the fast flux and the second M elements are the expansion coefficients for the thermal group. The matrices Λ and K have the form shown

$$\Lambda = \begin{bmatrix}
 \langle \psi_{1f}^* v_f^{-1} \psi_{1f} \rangle d/dt \dots \langle \psi_{1f}^* v_f^{-1} \psi_{5f} \rangle d/dt & 0 & 0 & 0 & 0 & 0 \\
 \langle \psi_{2f}^* v_f^{-1} \psi_{1f} \rangle d/dt \dots \langle \psi_{2f}^* v_f^{-1} \psi_{5f} \rangle d/dt & 0 & & & & 0 \\
 \dots & 0 & & & & 0 \\
 & 0 & & & & 0 \\
 \langle \psi_{5f}^* v_f^{-1} \psi_{1f} \rangle d/dt \dots \langle \psi_{5f}^* v_f^{-1} \psi_{5f} \rangle d/dt & 0 & & & & 0 \\
 0 & 0 & 0 & 0 & 0 & \langle \psi_{1T}^* v_T^{-1} \psi_{2T} \rangle d/dt \dots \langle \psi_{1T}^* v_T^{-1} \psi_{5T} \rangle d/dt \\
 0 & & & 0 & & \langle \psi_{2T}^* v_T^{-1} \psi_{2T} \rangle d/dt \dots \langle \psi_{2T}^* v_T^{-1} \psi_{5T} \rangle d/dt \\
 0 & & & 0 & & \dots \\
 0 & & & 0 & & \\
 0 & & & 0 & & \langle \psi_{5T}^* v_T^{-1} \psi_{2T} \rangle d/dt \dots \langle \psi_{5T}^* v_T^{-1} \psi_{5T} \rangle d/dt
 \end{bmatrix}$$

(4.28)

in Equations (4.28) and (4.29).

And

$$K = \begin{bmatrix} \begin{matrix} 5 \times 5 \\ \text{Submatrix} \\ B \end{matrix} & \begin{matrix} 5 \times 5 \\ \text{Submatrix} \\ C \end{matrix} \\ \begin{matrix} 5 \times 5 \\ \text{Submatrix} \\ D \end{matrix} & \begin{matrix} 5 \times 5 \\ \text{Submatrix} \\ E \end{matrix} \end{bmatrix} \quad (4.29)$$

where

$\psi_{if}^* = i^{\text{th}}$ fast adjoint space mode

$\psi_{iT}^* = i^{\text{th}}$ thermal adjoint space mode

$\psi_{jf} = j^{\text{th}}$ regular fast mode

$\psi_{jT} = j^{\text{th}}$ regular slow mode

$$B_{ij} = \left\langle \left(\frac{-d}{dx} \psi_{iF}^* \right) D_F \left(\frac{d}{dx} \psi_{jF} \right) - \psi_{iF}^* (\Sigma_R + D_F B^2) \psi_{jF} \right\rangle$$

$$C_{ij} = \left\langle \psi_{iF}^* \left\{ v \Sigma_f (1 - \beta) + \sum_{m=1}^H \lambda_m \beta_m \right. \right. \\ \left. \left. \times \int_{-\infty}^t v \Sigma_f(\tau) \exp[-\lambda_i(t-\tau)] d\tau \right\} \psi_{jT} \right\rangle$$

$$D_{ij} = \langle \psi_{iT}^* \Sigma_R \psi_{jF} \rangle$$

$$E_{ij} = \left\langle \left(\frac{-d}{dx} \psi_{iT}^* \right) D_T \left(\frac{d}{dx} \psi_{jT} \right) - \psi_{iT}^* (\Sigma_a + D_T B^2) \psi_{jT} \right\rangle .$$

and $\langle \rangle$ indicates integration over the reactor.

Reduction of Equation (4.27) to the form of Equation (4.8) for a white noise volume distributed fission source can be shown as follows.

The matrix K of Equation (4.29) can be written as

$$K = K(0) + \Delta K. \quad (4.30)$$

$K(0)$ represents the steady state matrix operator and ΔK represents its perturbation. The fluctuation in the fission sources are assumed to be due to the statistical variations in the number of neutrons per fission and thus ν is written

$$\nu = \nu(0) + \Delta \nu(t),$$

and, therefore, ΔK becomes

$$\Delta K = \begin{bmatrix} 0 & 5 \times 5 \\ \text{Submatrix} & \text{Submatrix} \\ & \Delta C \\ 0 & 0 \\ \text{Submatrix} & \text{Submatrix} \end{bmatrix} \quad (4.31)$$

where

$$\begin{aligned} \Delta C_{ij} = & \langle \psi_{if}^* \Sigma_f (1-B) \psi_{jT} \rangle_2 \Delta \nu_2(t) \\ & + \langle \psi_{if}^* \Sigma_f (1-B) \psi_{jT} \rangle_4 \Delta \nu_4(t) \\ & + \langle \psi_{if}^* \Sigma_f \psi_{jT} \rangle_2 \sum_{m=1}^H \lambda_m \beta_m \times \int_{-\infty}^t \Delta \nu_2(\tau) \exp[-\lambda_m(t-\tau)] d\tau \end{aligned}$$

$$+ \langle \psi_{if} \Sigma_f \psi_{jt} \rangle_4 \sum_{m=1}^M \lambda_m \beta_m \times \int_{-\infty}^t \Delta v_4(\tau) \exp[-\lambda_m(t-\tau)] d\tau .$$

The subscripts 2 and 4 refer to the two fuel regions in the reactor. Due to the perturbation ΔK , the expansion coefficients vary about their steady-state value and may be expressed as

$$A(t) = A(0) + \Delta A(t) . \quad (4.32)$$

Substitution of Equations (4.30) and (4.32) into (4.27) yields

$$\Lambda[A(0) + \Delta A(t)] = [K(0) + \Delta K][A(0) + \Delta A(t)]$$

$$\begin{aligned} \Lambda A(0) + \Lambda \Delta A(t) &= K(0)A(0) + K(0)\Delta A(t) + \Delta K A(0) \\ &+ \Delta K \Delta A(t) . \end{aligned} \quad (4.33)$$

Since $\Delta K \Delta A$ is a small term one can neglect it. Noting $\Lambda A(0) = 0$ and using the steady state condition $K(0)A(0) = 0$ one can reduce Equation (4.33) to the form

$$\Lambda \Delta A \approx K(0)\Delta A(t) + \Delta K A(0) . \quad (4.34)$$

Equation (4.34) has the form of Equation (4.8) where

$$D = \Lambda - K(0) \quad (4.35)$$

and

$$F(t) = \Delta K A(0) .$$

The space modes are chosen such that

$$\phi(x,0) = \sum_{i=1}^5 \psi_i(x),$$

and therefore

$$A(0) = \text{Col } [1 \ 1 \ 1 \ \dots \ 1] .$$

Since the elements of $A(0)$ are unity, each element of F will be given by the sum of the elements of each row in ΔK . Therefore

$$F_i = \sum_{j=1}^5 \Delta C_{ij} \quad i=1,2,\dots,5 \quad (4.36)$$

and

$$F_{i+5} = 0 \quad i=1,2,\dots,5$$

where ΔC_{ij} is the general element in Submatrix C in Equation (4.31).

Substitution of the matrix elements of F , $\Delta K A(0)$, into Equation (4.11) yields the input correlation matrix elements χ_{mn} , which have the form

$$\chi_{mn}(\xi) = \left[\sum_{j=1}^5 \Delta C_{ij}(t) \right] \left[\sum_{i=1}^5 \Delta C_{ij}(t+\xi) \right] . \quad (4.37)$$

Fourier transforming this matrix one gets the input spectral density matrix $\hat{\chi}(\omega)$ with elements

$$\hat{\chi}_{mn}(\omega) = \left[\left(\sum_{j=1}^5 \langle \psi_{mF}^* \psi_{jT} \rangle_2 \right) \left(\sum_{j=1}^5 \langle \psi_{nF}^* \psi_{jT} \rangle_2 \right) \right] \quad (4.38)$$

$$\begin{aligned}
& + \left(\sum_{j=1}^5 \langle \psi_{mF} \psi_{jT} \rangle_4 \right) \left(\sum_{j=1}^5 \langle \psi_{nF} \psi_{jT} \rangle_4 \right) \\
& \times \left\{ [\Sigma_f (1-\beta)]^2 + 2 \Sigma_f^2 (1-\beta) \sum_{i=1}^H \frac{\lambda_i^2 B_i}{(\lambda_i^2 + \omega^2)} + \Sigma_f^2 \sum_{i=1}^H \frac{\lambda_i^2 \beta_i}{(\lambda_i^2 + \omega^2)} \right\} \Delta \bar{v}
\end{aligned}$$

where $m, n=1, 2, \dots, 5$ and $\Delta \bar{v}$ is an amplitude factor. Equation (4.38) is based on the assumption that $\Delta v(t)$ has the characteristics of white noise and the same amplitude factor in each fuel region. The elements of $\hat{\chi}$ not assigned values by Equation (4.38) are zero. The matrix D of Equation (4.35) is obtained from Equations (4.28) and (4.29). The matrix \hat{D} of Equation (4.24) is obtained by Fourier transforming Equation (4.35). In this transformation the time derivative operator is replaced with $j\omega$ and the integral operator with

$$v \Sigma_f \sum_{i=1}^H \frac{\lambda_i \beta_i}{\lambda_i + j\omega}.$$

The resulting expression for \hat{D} is

$$\hat{D} = \begin{bmatrix} \text{Submatrix } \hat{B} & \text{Submatrix } \hat{C} \\ 5 \times 5 & 5 \times 5 \\ \text{Submatrix } \hat{E} & \text{Submatrix } \hat{H} \\ 5 \times 5 & 5 \times 5 \end{bmatrix} \quad (4.39)$$

where

$$\begin{aligned}\hat{B}_{ij} = & \langle \psi_{iF}^* v_F^{-1} \psi_{jF} \rangle j\omega - \langle \left(\frac{-d}{dx} \psi_{iF}^* \right) (D_F \frac{d}{dx} \psi_{jF}) \\ & - \psi_{iF}^* (\Sigma_R + D_F B^2) \psi_{jF} \rangle\end{aligned}$$

$$\hat{C}_{ij} = -\langle \psi_{iF}^* [\nu \Sigma_F (1-\beta) + \nu \Sigma_f \sum_{i=1}^M \frac{\lambda_i \beta_i}{\lambda_i + j\omega}] \psi_{jT} \rangle$$

$$\hat{E}_{ij} = -\langle \psi_{iT}^* \Sigma_R \psi_{jF} \rangle$$

$$\begin{aligned}\hat{H}_{ij} = & \langle \psi_{iT}^* v_T^{-1} \psi_{jT} \rangle j\omega - \langle \left(\frac{-d}{dx} \psi_{iT}^* \right) (D_T \frac{d}{dx} \psi_{jT}) \\ & - \psi_{iT}^* (\Sigma_a + D_T B^2) \psi_{jT} \rangle\end{aligned}$$

$$i, j = 1, 2, \dots, 5$$

ω = frequency in rad/sec

$$j = \sqrt{-1}.$$

The delayed neutrons were approximated by one average group having a decay constant λ of 0.08 sec^{-1} and a delayed fraction β of 0.0064. After finding all the elements for the matrices of Equation (4.24), the equation was solved for the elements Γ_{ij} using the IBM-360 digital computer. The auto-spectral-density functions at space points 1=center of region 2, 2=10 cm to the right of region 2, 3=center of the

reactor, 4=center of region 4 and 5=20 cm to the right of region 4 were calculated and shown for some reactor configurations in the following section. The magnitude of the cross-spectral density functions and the coherence functions between points 1-1, 1-2, 1-3, 1-4 and 1-5 were calculated and are shown in the next section.

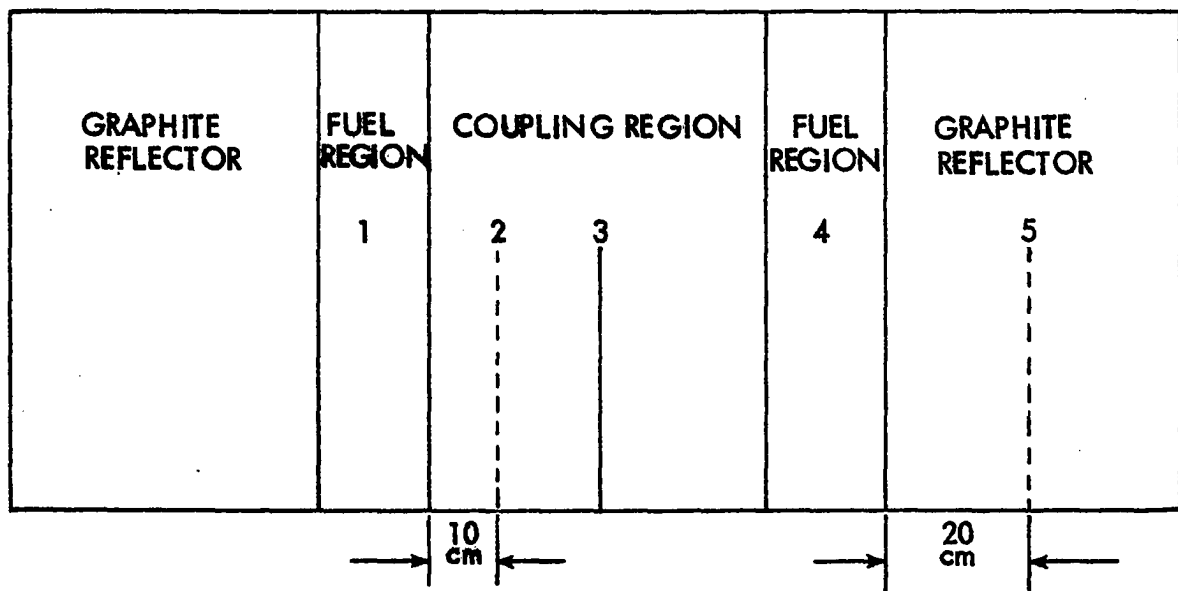


Figure 4.1. Space points 1,2,3,4 and 5 with coupling region change in thickness and nuclear parameters

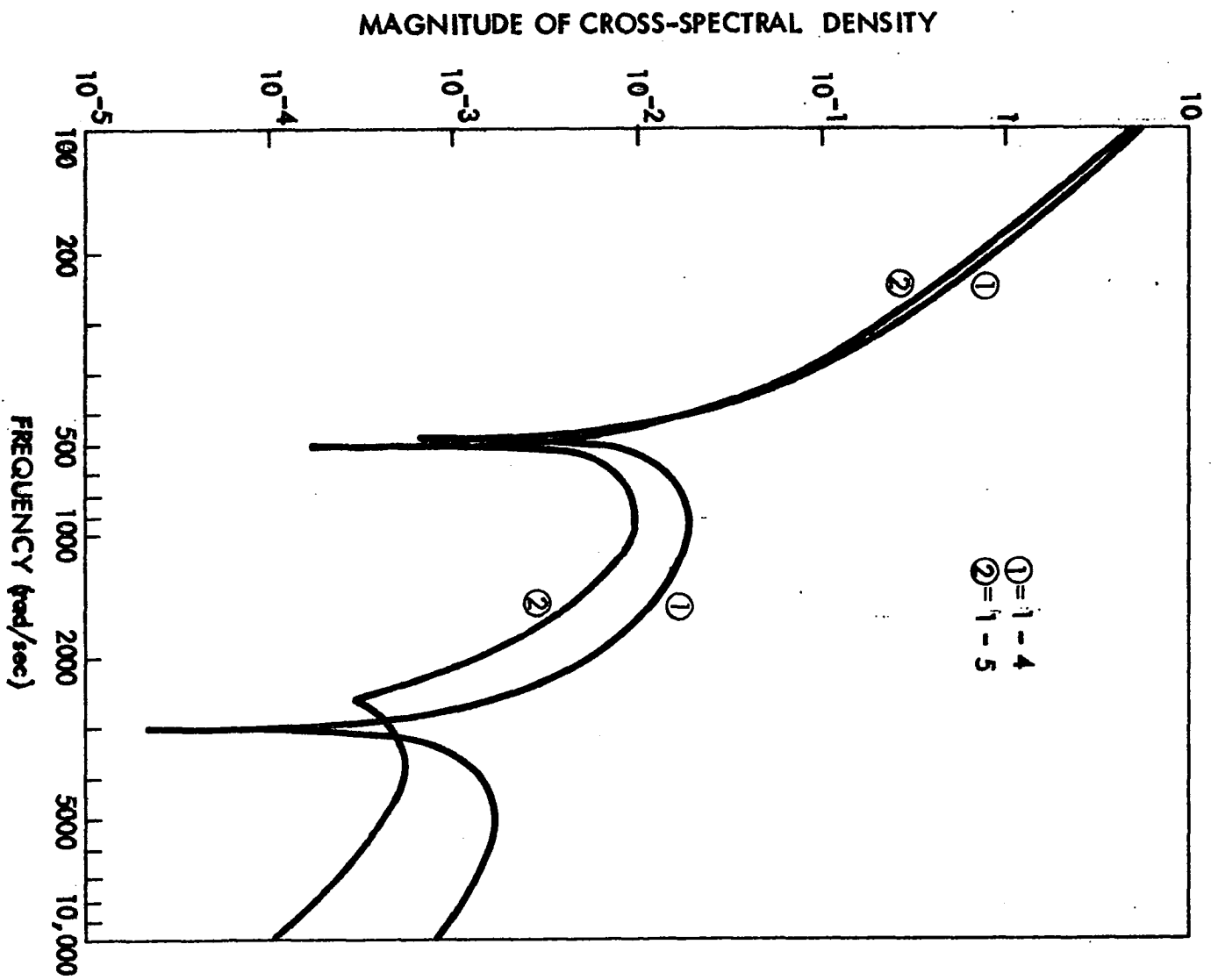
V. APPLICATION OF NOISE MODEL AND RESULTS

In this section the results obtained from the application of the space-dependent noise model described in section 4 are presented. The auto-spectral-density functions (ASDF) for space points 1 to 5 and the cross-spectral-density functions (CSDF) between space points 1 and space points 1 to 5 of Figure 4.1 have been obtained for the coupling region sizes and materials described in section 3.

Typical results obtained for the magnitude of the CSDF are shown in Figure 5.1 for the CSDF. These solutions are for a 45 cm graphite coupling region. The space dependence, which becomes more significant with increasing frequency, is apparent in that figure.

It will be noted that the CSDF for space points 1-4 and 1-5 exhibit the characteristic "sink" or "null" frequency that has been experimentally observed in coupled core argonaut reactors (13, 3). It should be noted that only the first or lowest frequency sink has been observed experimentally. There is some evidence based on a space-dependent frequency response model investigated by Nodean (23) that the modal analysis technique used in this investigation results in an exaggerated high frequency sink. Unless specifically noted, the term sink frequency will be assumed to

Figure 5.1. Relative magnitude of cross-spectral density function, Φ_{1-4} and Φ_{1-5} , for 45 cm graphite coupling region



apply only to the experimentally observed low frequency sink in the remainder of this thesis. Nodean (23) found for example that for a 45 cm coupling region the sink appeared as an inflection point in the magnitude curve. As the coupling region size was increased to 75 cm a small sink developed but it was not as pronounced as those shown here.

In the case of a symmetric reactor the CSDF for space points 1-4 is real and the sink frequency is a true null frequency. It exists when the real part of the CSDF vanishes. For space points 1-5 the CSDF is complex and the sink frequency is not a true null frequency since it can have an imaginary component at the zero of the real part.

Since the major point of interest in this thesis is the effects of the characteristics of the coupling region on the sink frequency, results for space points 1-4 and 1-5 will be of primary interest for the other cases studied. It might be noted that the sink characteristics were not observed for the other space points for any of the coupling regions investigated. The sink frequencies were found to be sensitive to the thickness of the coupling region. Figure 5.2 shows the magnitude of the CSDF between points 1-4 and 1-5 for a reactor with a 25 cm graphite coupling region. As can be seen no sink exists but inflection in the curve. Figure 5.3 shows the magnitude of the CSDF between points 1-4 and 1-5 for a reactor with 40 cm graphite coupling region. Figure

Figure 5.2. Relative magnitude of cross-spectral density function, ϕ_{1-4} and ϕ_{1-5} , for 25 cm graphite coupling region

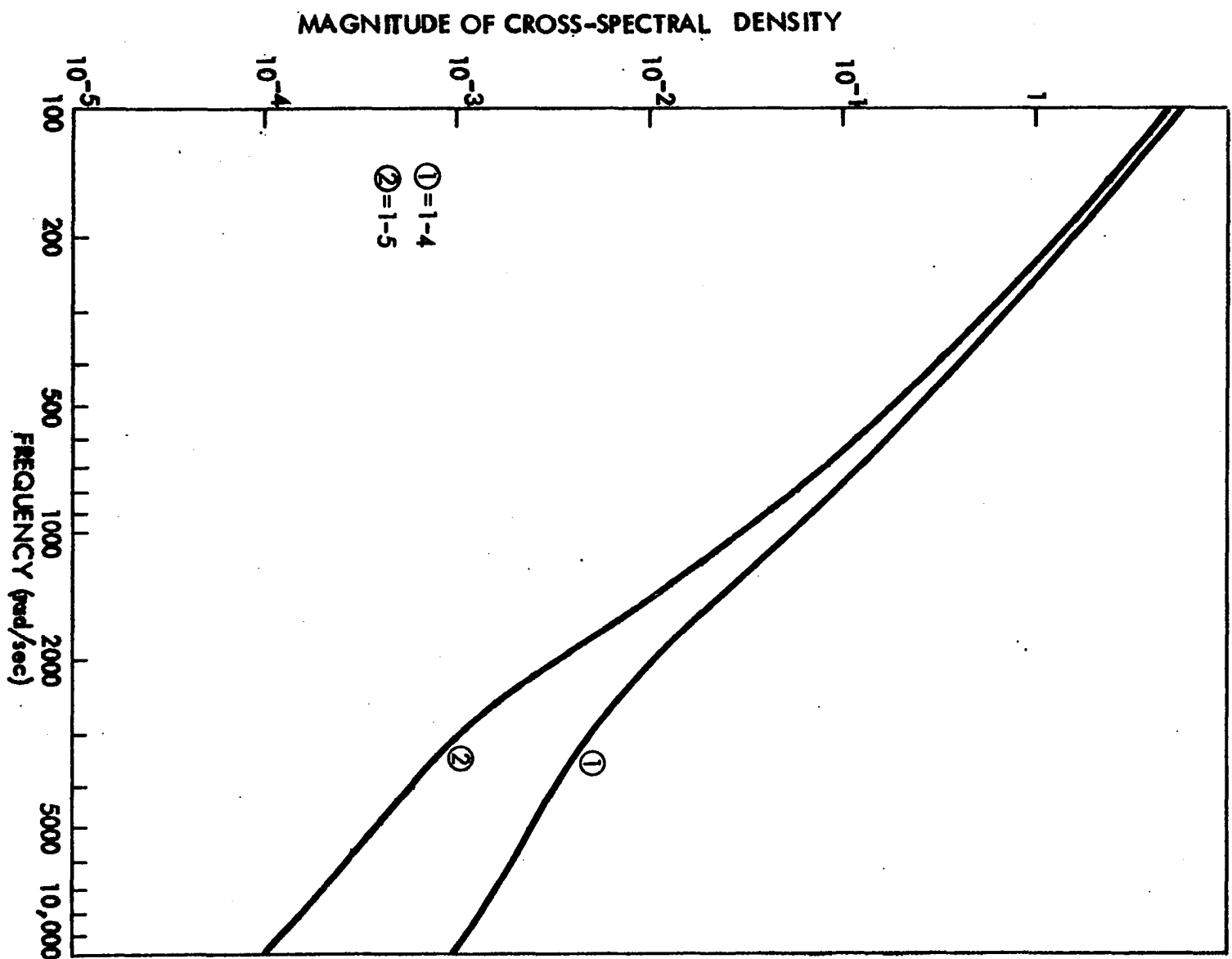
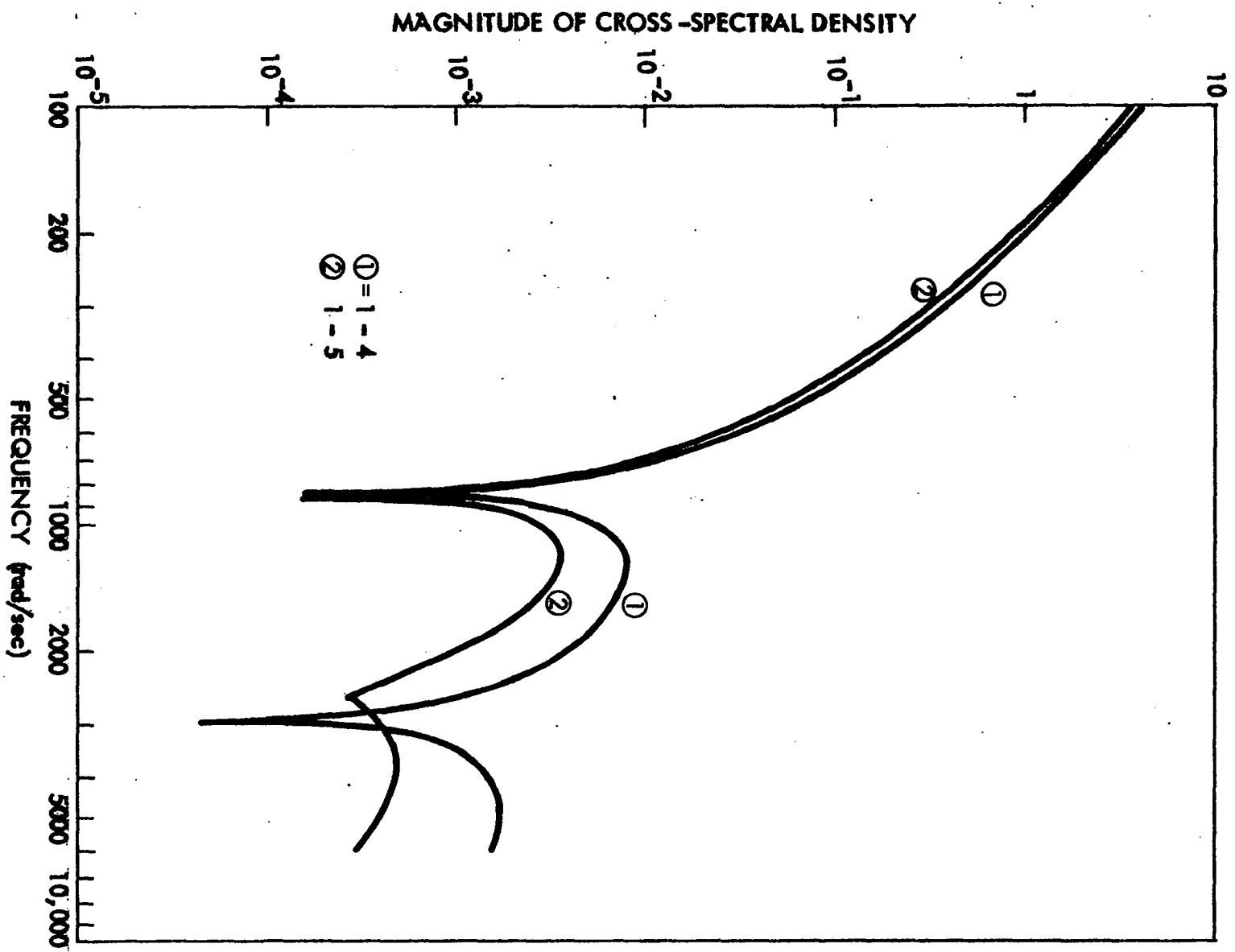


Figure 5.3. Relative magnitude of cross-spectral density function, Φ_{1-4} and Φ_{1-5} , for 40 cm graphite coupling region



5.4 shows the two sinks for the CSDF for a 75 cm graphite coupling region. From the figure it can be seen that the first sink has moved to a lower frequency than the case of the 40 cm coupling region. The second sink has been found to be much less sensitive to coupling region size than that of the first sink.

Table 5.1 shows the frequencies at which the first, s_1 , and the second, s_2 , sinks occur for different coupling region sizes of graphite.

Table 5.1. Sink frequency as a function of core space for a graphite coupling region

Coupling region thickness cm	s_1 (1-4) rād/sec	s_2 (1-4) rād/sec	s_1 (1-5) rād/sec	s_2 (1-5) rād/sec
25	-	-	-	-
35	1500	2400	1450	2300
40	840	2950	865	2600
45	580	3000	600	2500
55	345	1900	360	1400
75	160	2525	175	2100
85	100	2550	109	2150

Looking at Table 5.1 it can be seen that the first sink is very sensitive to the coupling region width and the frequency at which it occurs decreases with increased coupling region size. Figure 5.5 shows a plot of the first sink frequency

Figure 5.4. Relative magnitude of cross-spectral density function, ϕ_{1-4} and ϕ_{1-5} , for 75 cm graphite coupling region

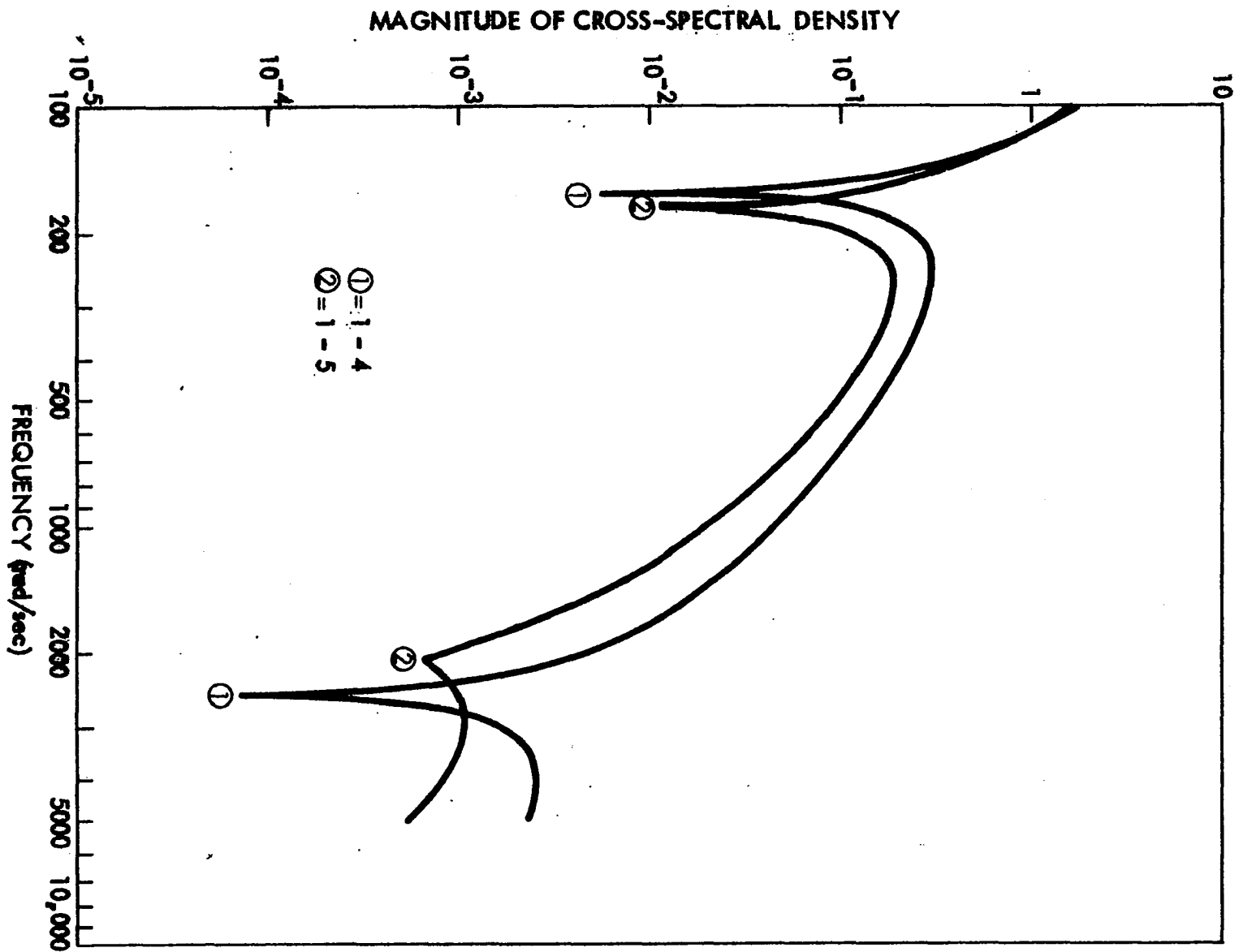
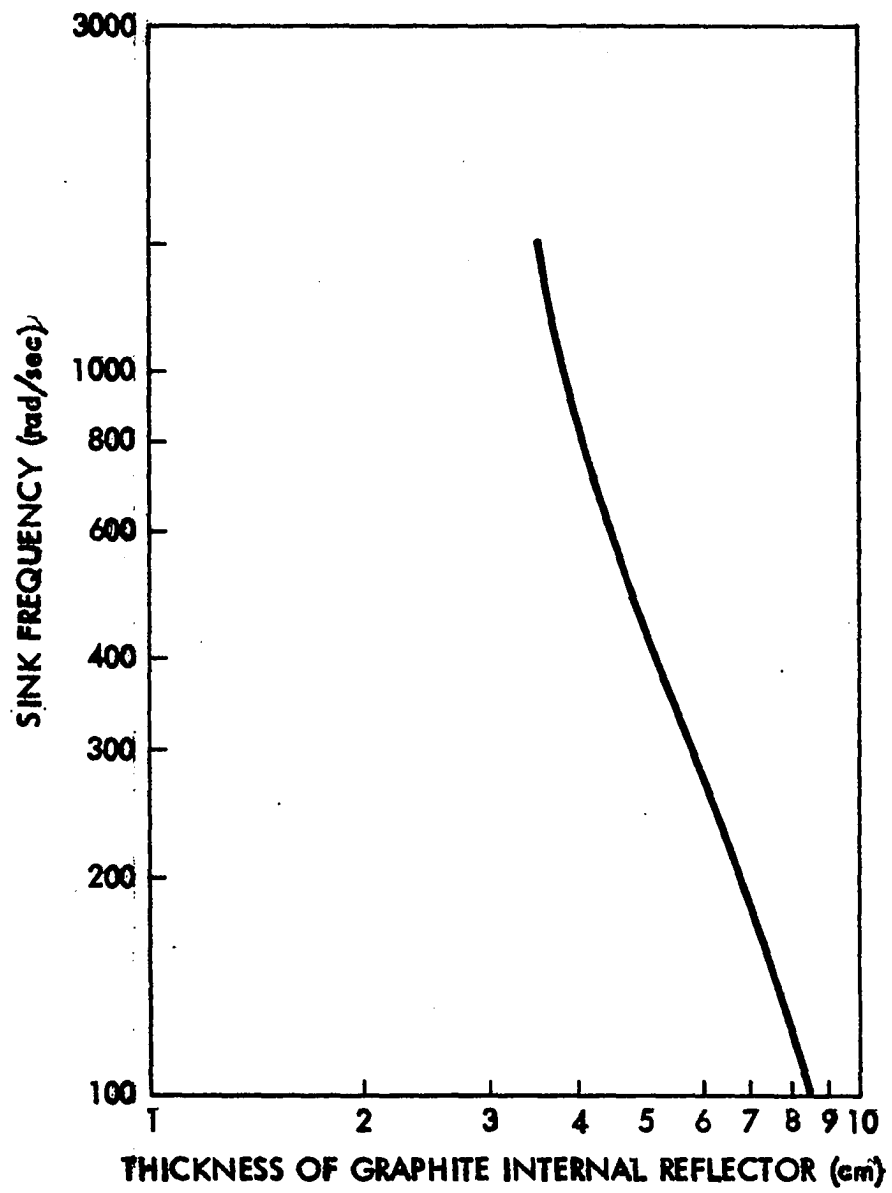


Figure 5.5. First sink frequency of cross-spectral density function, ϕ_{1-4} , for different thicknesses of graphite coupling region



versus coupling region size for space points 1-4. Figure 5.6 shows the magnitude of the CSDF when different thickness of heavy water are used as an internal reflector.

Table 5.2 shows the sink frequencies for different thicknesses of heavy water as an internal reflector.

Table 5.2. Sink frequency as a function of spacing between cores for heavy water coupling region

Coupling region thickness cm	$s_1(1-4)$ rad/sec	$s_2(1-4)$ rad/sec	$s_1(1-5)$ rad/sec	$s_2(1-5)$ rad/sec
20	5000	-	5600	-
25	1600	7000	1700	5000
35	560	8200	630	4800
45	260	7500	300	4400
55	110	6800	130	3600
75	0.17	5400	000.2	2900

Looking at Table 5.2 and at Figure 5.6 the behavior of the first sink frequency as a function of coupling region size can be seen. It is to be noted that the rate of decrease of the sink frequency is very high at strong and weak coupling and the rate decreases at intermediate coupling. Figure 5.8 shows the magnitude of the ASDF at points 1, 2, 3, 4 and 5 for 45 cm heavy water as an internal reflector. The space dependence of the function is more pronounced at high frequency since at low frequency the value of the function

Figure 5.6. Relative magnitude of cross-spectral density function, Φ_{1-4} , for different thicknesses of heavy water coupling region

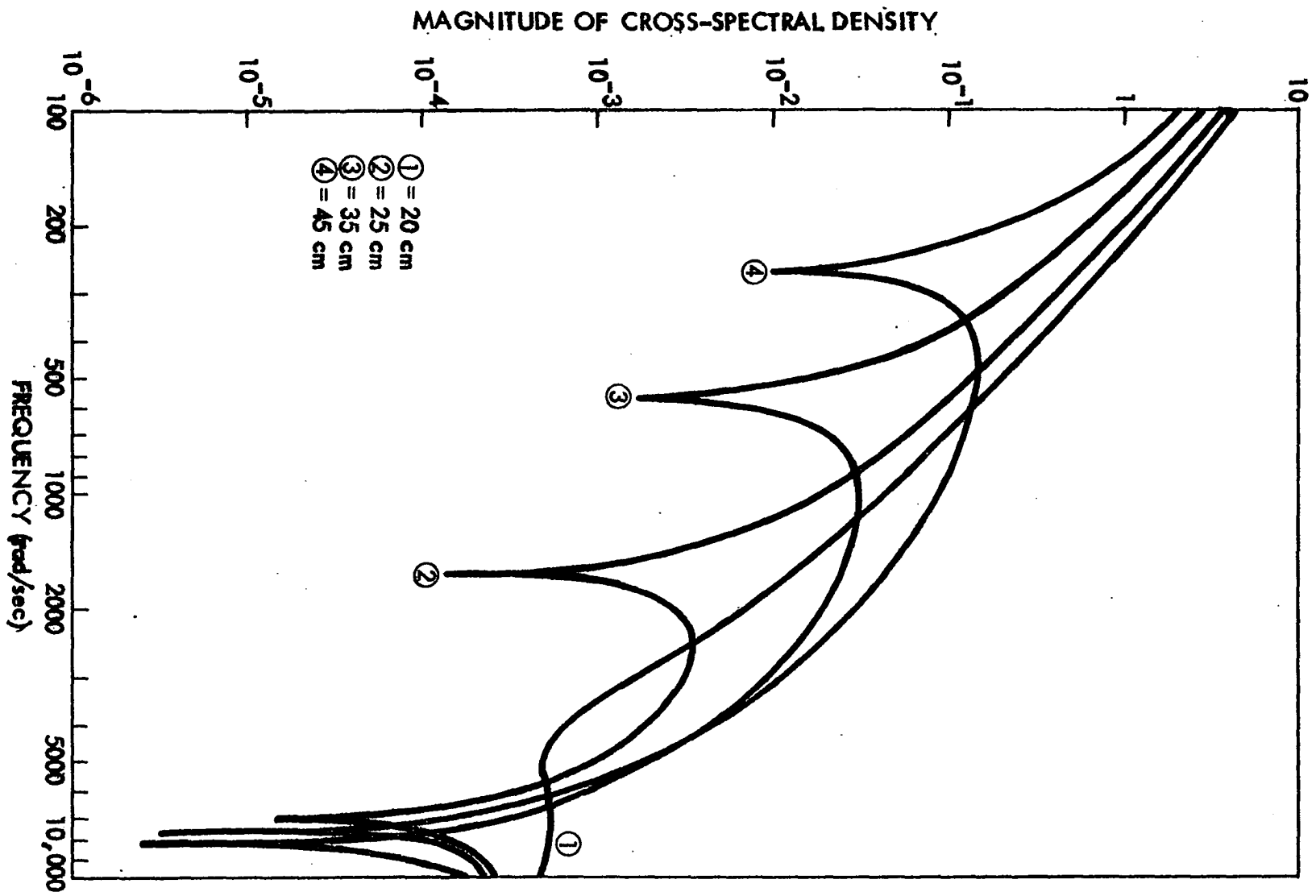


Figure 5.7. First sink frequency of cross-spectral density functions, ϕ_{1-4} and ϕ_{1-5} , for different thicknesses of heavy water coupling region

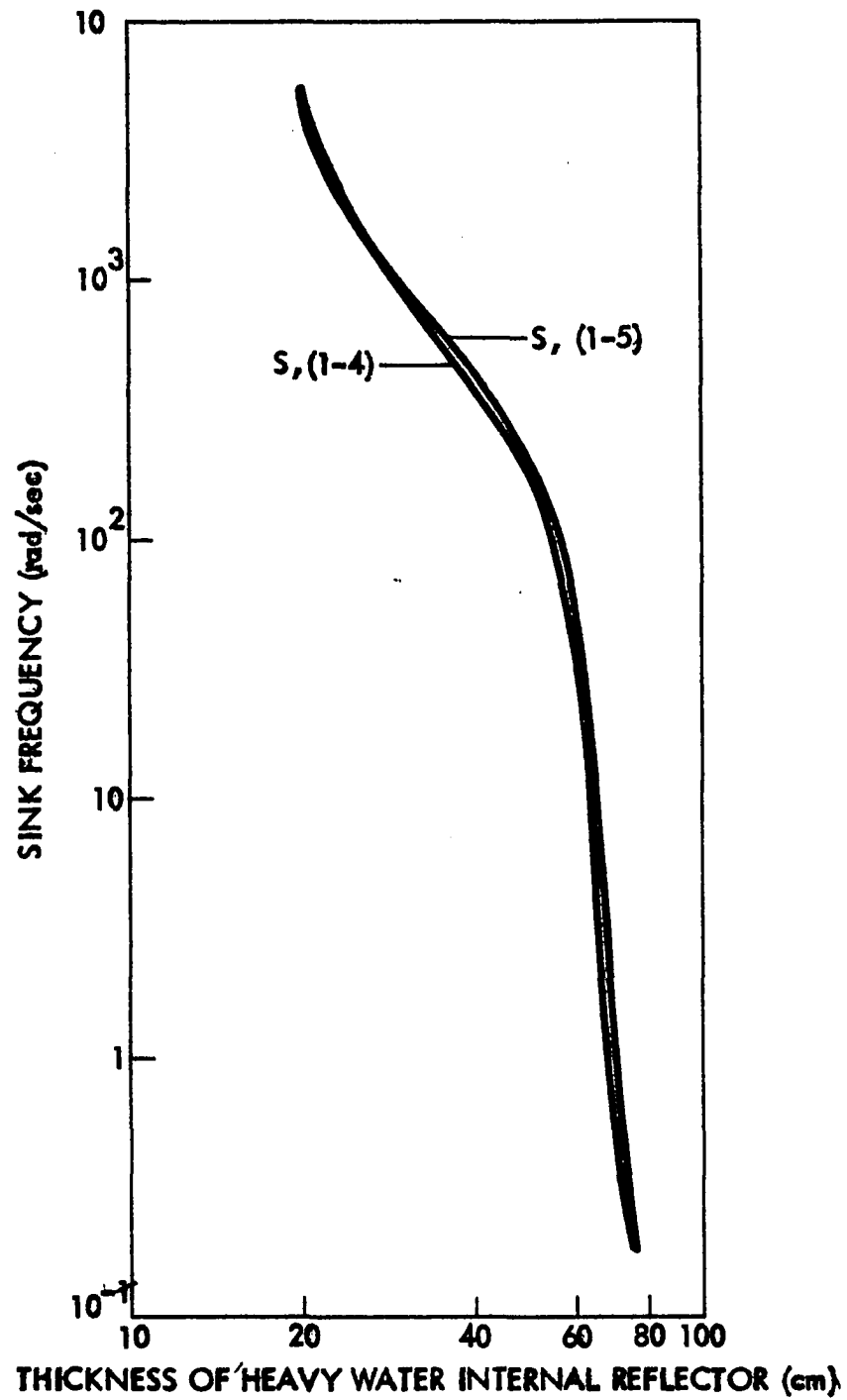
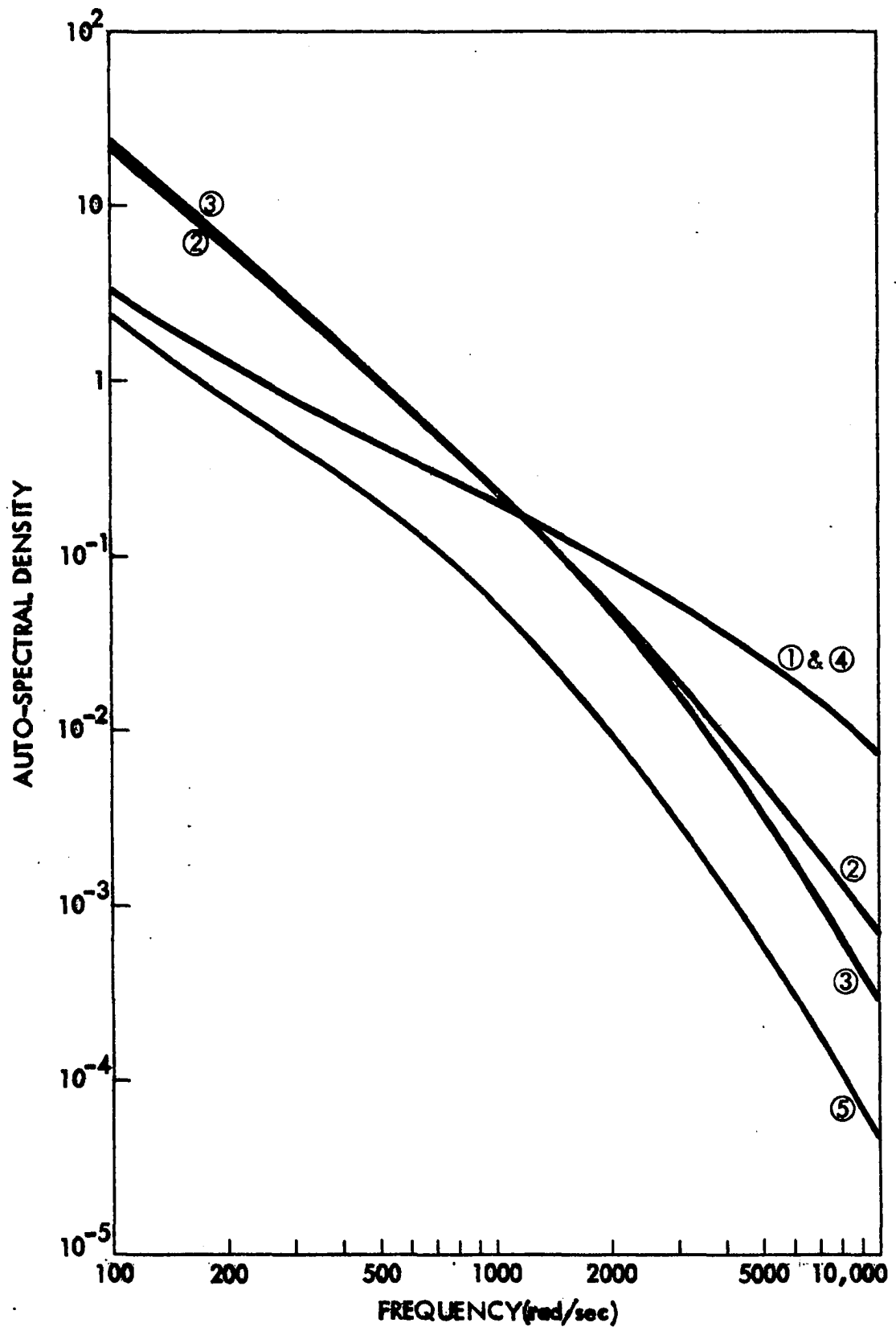


Figure 5.8. Relative magnitude of auto-spectral density function at points 1, 2, 3, 4 and 5 for 45 cm heavy water coupling region



is still dominated by the steady state distribution of the flux.

Figure 5.9 shows the CSDF for a 45 cm heavy water coupling region for points 1-1, 1-2, 1-3, 1-4 and 1-5. These curves tend to show how the sink develops with increasing distance between points of cross correlation. Figure 5.10 shows a plot of the phase angle of the CSDF shown in Figure 5.9. From Figure 5.10 it can be seen that the phase angle of the CSDF plays an important role in the existence of the sink. For the 1-4 case it has been found that a phase shift of 180° occurs at the two sink frequencies. For the 1-5 case a phase shift of 270° occurred at the first sink and 180° phase shift occurred at the second sink frequency. For the 1-1 case the phase angle is zero for all frequencies which shows that it is also a real function as expected. For the 1-2 and 1-3 cases there is a small phase angle observed and there is no jump in the phase angle, in these two cases no sinks were observed in the magnitude of the CSDF.

Figure 5.11 shows the coherence function for a 45 cm heavy water as an internal reflector. As shown from Figure 5.11 the coherence function has the same sinks as the CSDF but the space dependence is more enhanced in the coherence function more than that of the CSDF. Effects of the removal cross section on the magnitude and zeros (sinks) of the

Figure 5.9. Relative magnitude of cross-spectral density function, Φ_{1-1} , Φ_{1-2} , Φ_{1-3} , Φ_{1-4} and Φ_{1-5} , for 45 cm heavy water coupling region

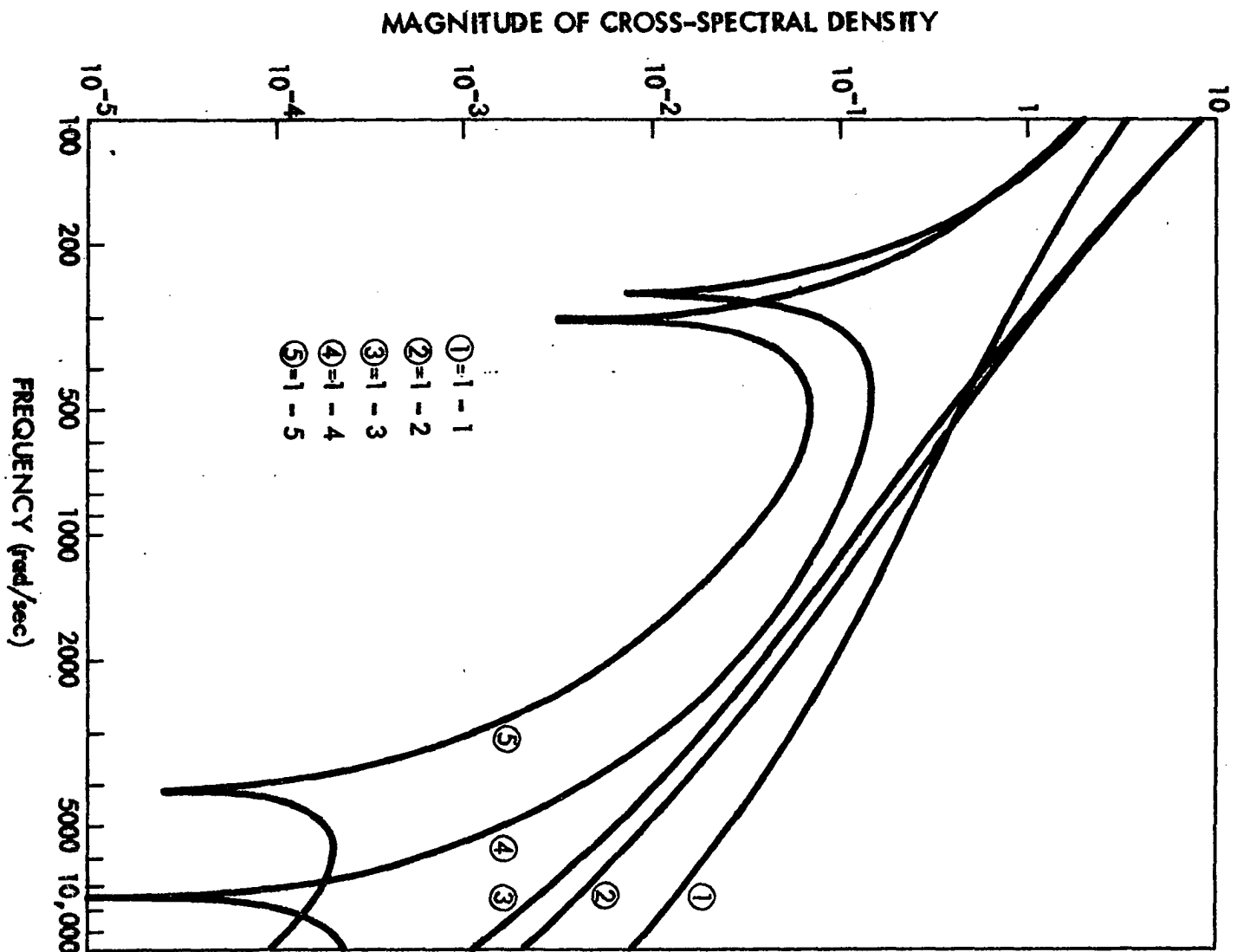


Figure 5.10. Phase angle of cross-spectral density function,
 ϕ_{1-1} , ϕ_{1-2} , ϕ_{1-3} , ϕ_{1-4} and ϕ_{1-5} , for 45 cm heavy
water coupling region

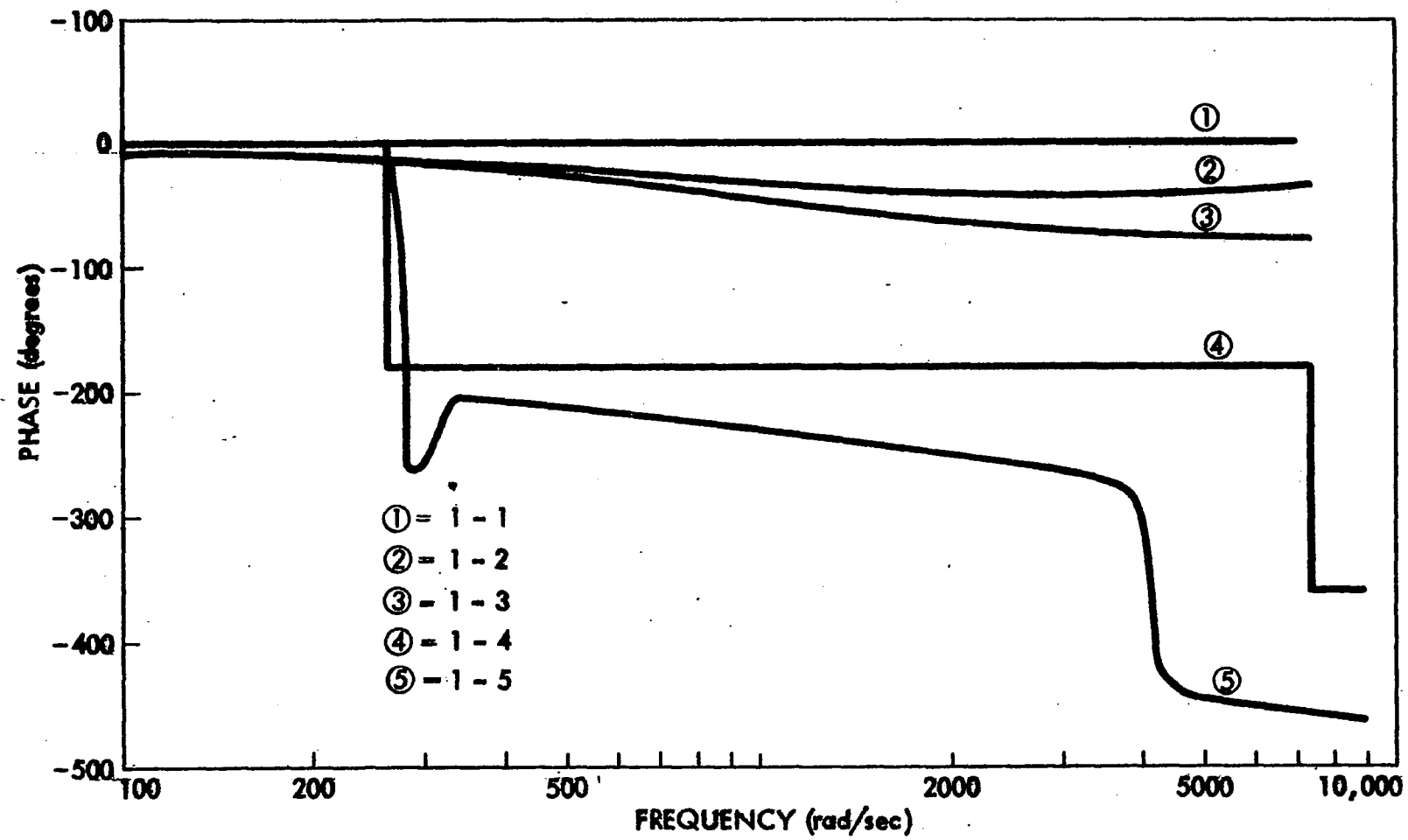
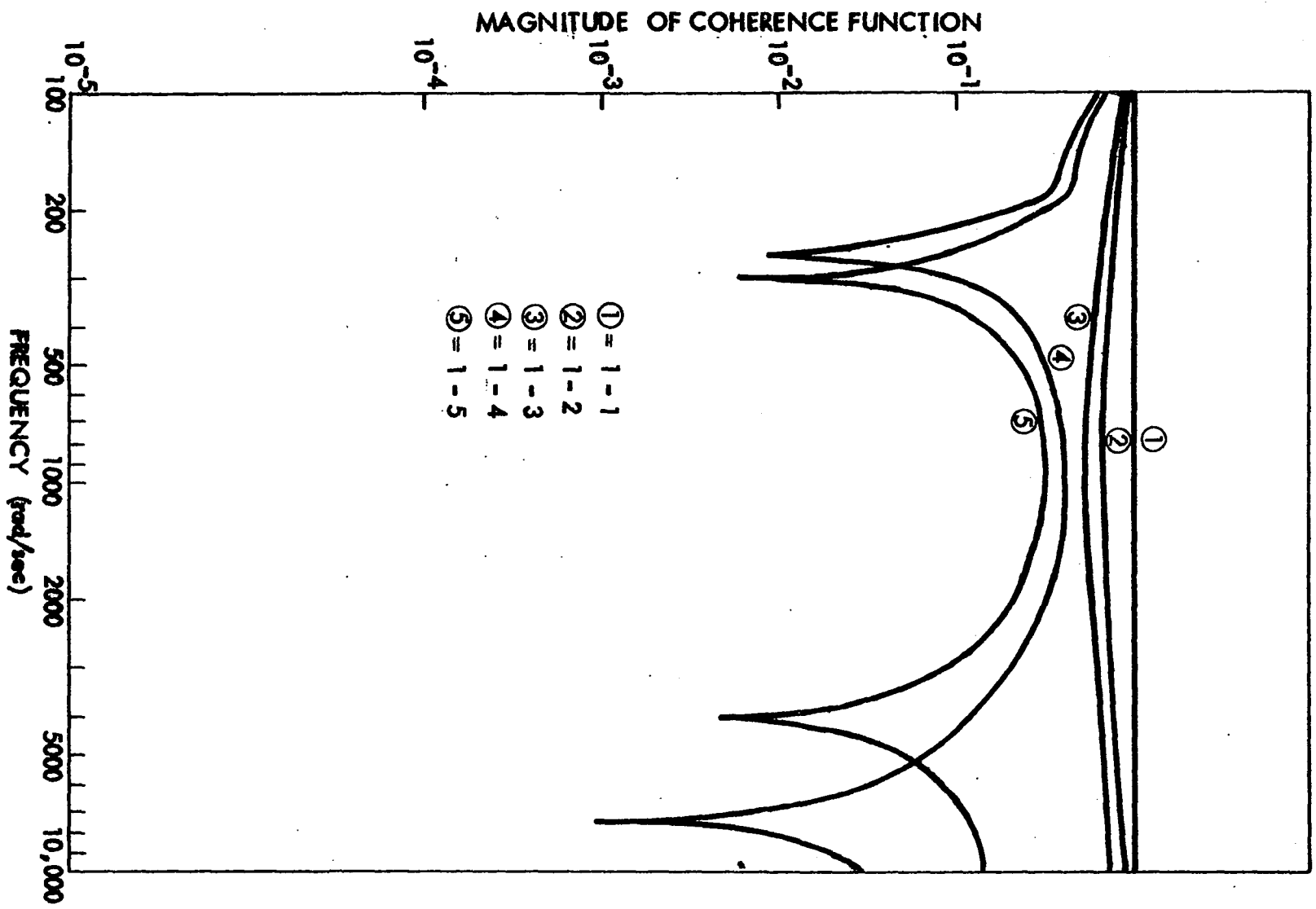


Figure 5.11. Relative magnitude of coherence function,
 R_{1-1} , R_{1-2} , R_{1-3} , R_{1-4} and R_{1-5} , for 45 cm
heavy water coupling region



CSDF for space points 1-4 are shown in Figure 5.12 for a 45 cm internal reflector. The other nuclear constants of this figure are those of heavy water. From that figure it can be seen that both the first and second sinks are very sensitive to the removal cross section. A plot of the first and second sink frequencies is shown on Figure 5.13. Both sinks show a linear relation on log paper, but the second sink shows a positive slope.

Figure 5.14 shows a plot of the first sink frequency of the 1-4 case as a function of the absorption cross section of the coupling material (all the other nuclear parameters are those of heavy water).

The magnitude of the CSDF between points 1-4 and 1-5 for a 45 cm beryllium coupling region is shown in Figure 5.15.

As previously mentioned, experimental evidence of the existence of the first sink was demonstrated by Hendrickson (13) for the UTR-10 reactor. Albrecht and Seifritz (3) measured the sink frequency of the CSDF between the two cores (equivalent to ϕ_{1-4} in this work) of the Argonaut reactor at Karlsruhe. This reactor has 42 cm thick graphite coupling region. A sink was found at approximately 700 rad/sec.

From Figure 5.5 it can be predicted that for 42 cm graphite a sink frequency should exist at 720 rad/sec which agrees well with Albrecht's experimental results. In their

Figure 5.12. Relative magnitude of cross-spectral density function, ϕ_{1-4} , for three different removal cross sections with the other nuclear parameters are equal to those of 45 cm heavy water coupling region

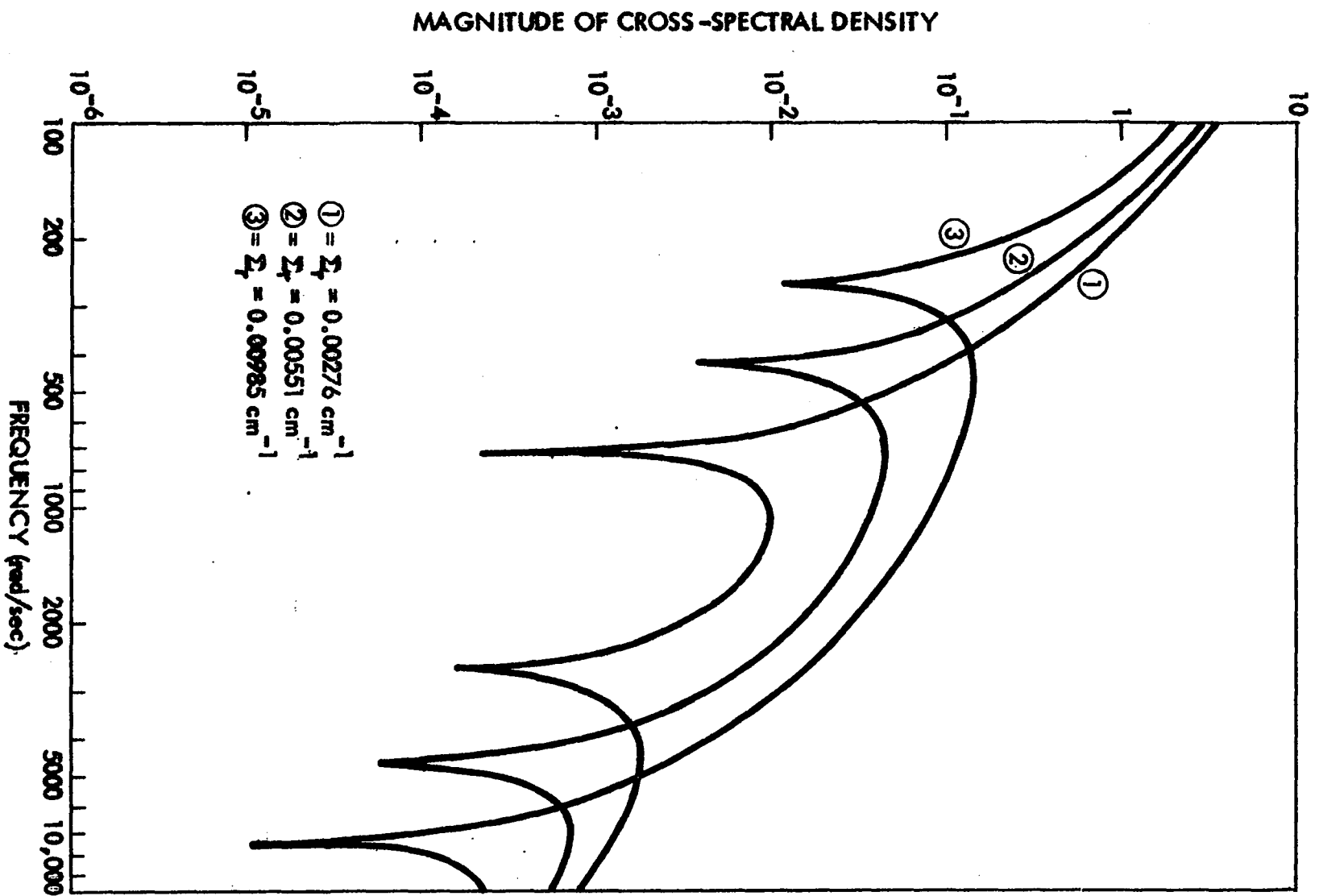


Figure 5.13. First and second sink frequency of Figure 5.11 as a function of removal cross section

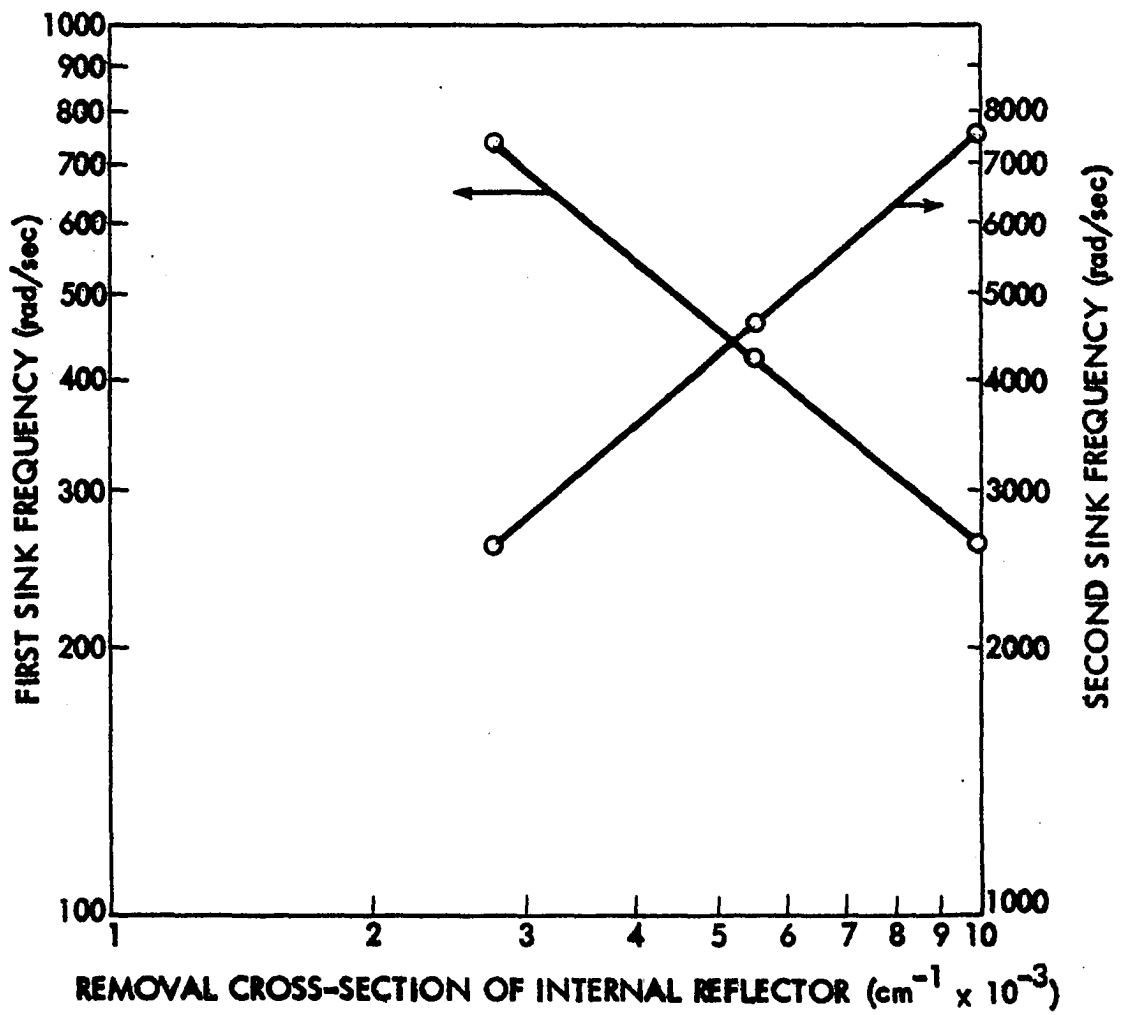


Figure 5.14. Effect of absorption cross section of coupling region on first sink frequency of ϕ_{1-4}

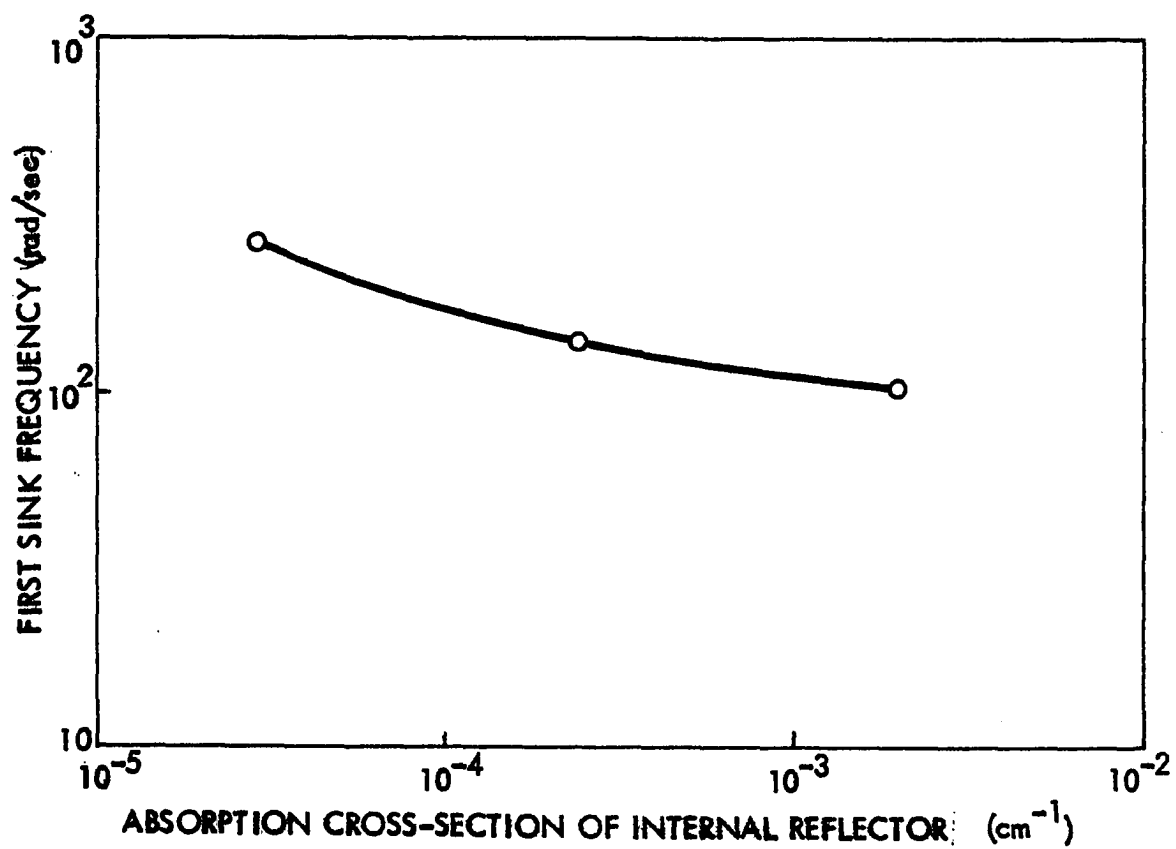
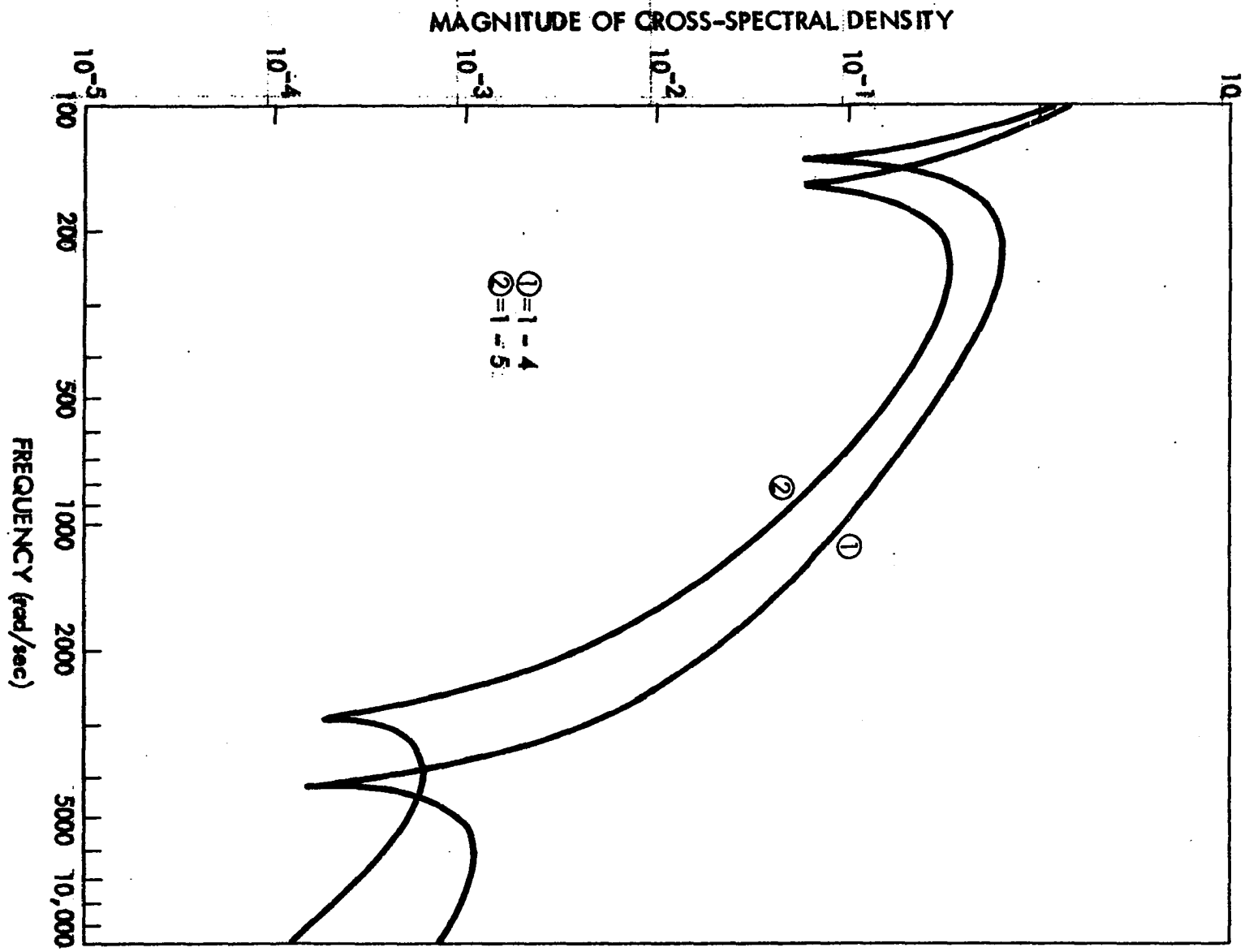


Figure 5.15. Relative magnitude of cross-spectral density function, Φ_{1-4} and Φ_{1-5} , for 45 cm beryllium internal reflector



mathematical model, Albrecht and Seifritz treated the reactor as a symmetrical two node system which is equivalent to the 1-4 case in the continuous system used in this thesis.

Albrecht and Seifritz (3) showed that the frequency dependence of the coherence function, which has the same zeros as the CSDF, is wholly dependent on the characteristics of the coupling transfer function $K(\omega)$. This is defined for two node reactor as the ratio of the Laplace transform of the response from one node divided by the Laplace transform of the response from the other node when a perturbation is introduced only in the node appearing in the denominator. The two node system as described by Albrecht and Seifritz (2) is shown as the block diagram of Figure 5.16.

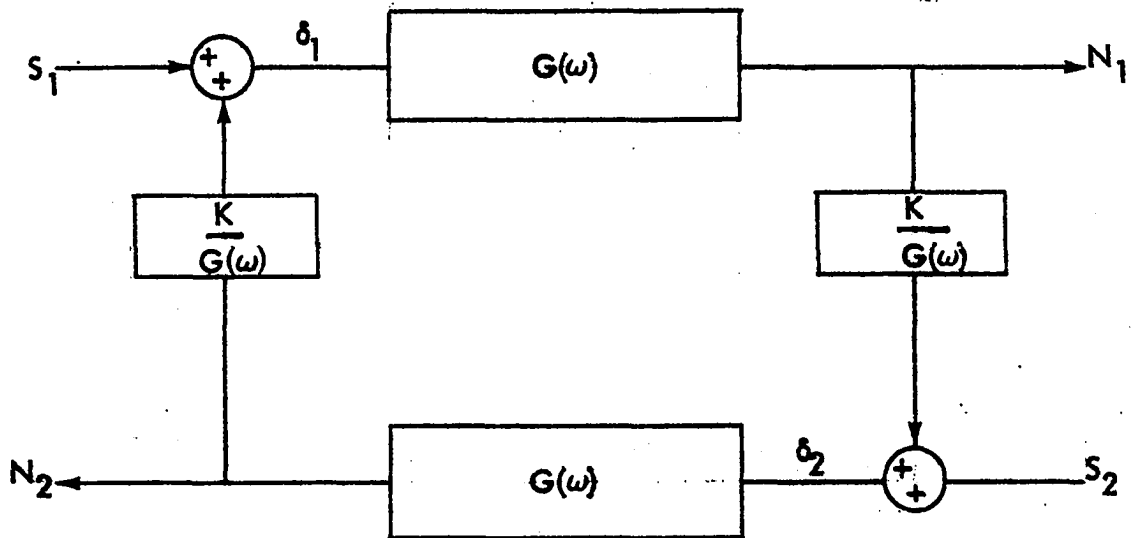


Figure 5.16. Block diagram for symmetric two node system

According to Figure 5.16, $G(\omega)$ is an arbitrary nodal transfer function and K is an arbitrary coupling function. An expression of the coherence function for this system was given as

$$R(\omega) = \frac{2 \operatorname{Re} K}{1 + |K|^2} \quad (5.1)$$

which shows that the zero of the coherence function (and for the CSDF) exists at the frequency at which the real part of coupling transfer function vanishes, i.e. where the coupling function has a phase of 90° . Since in this symmetric case $R(\omega)$ is real, then a zero means a crossing from the positive to the negative real axis. Using this model it can be seen that the sink frequency depends on the form of K . In a two node symmetric reactor $K(\omega)$ has the form (3)

$$\begin{aligned} K &= \frac{\varepsilon}{\Lambda} \frac{p(j\omega)}{j\omega + \frac{\beta - \rho}{\Lambda}} \\ &= \frac{\varepsilon}{\Lambda} \frac{p(j\omega) (-j\omega + \frac{\beta - \rho}{\Lambda})}{\omega^2 + (\frac{\beta - \rho}{\Lambda})^2} \end{aligned} \quad (5.2)$$

where

ε = the coupling reactivity

Λ = finite neutron life time

p = normalized density function for delay times

ρ = reactivity of each subcritical zone

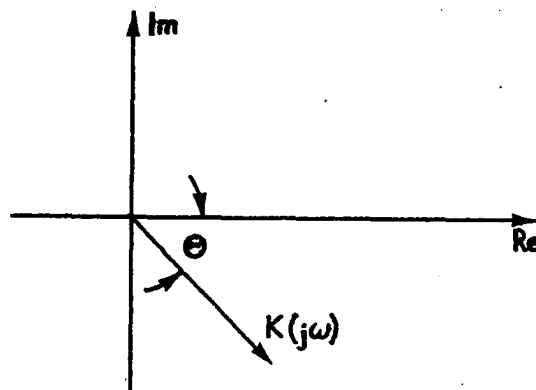
The time delay function accounts for the time delay required for a neutron disturbance to propagate from one core to the other. Several forms for the time delay function have been suggested (3). Two of the more interesting are

$$p(t) = \delta(t-\tau) \qquad p(j\omega) = e^{-j\omega\tau}$$

and

$$p(t) = \frac{1}{\tau_0} e^{-\frac{t}{\tau_0}} \qquad p(j\omega) = \frac{1}{1+j\omega\tau_0}$$

It is clear that the sink frequency depends upon the form of $p(j\omega)$. Note $K(\omega)$ is a complex number and can be shown on the complex plane as follows



It can be seen that the real part of K vanishes when θ is -90° and therefore the sink occurs when the phase of the coupling transfer function is -90° . In this two node system the phase shift in the coherence function comes from two sources (1) the reactor node $1/(j\omega + \frac{\beta-\rho}{\Lambda})$ and (2) the time delay function $p(j\omega)$. The reactor phase shift $\theta_R = \frac{1}{j\omega + (\frac{\beta-\rho}{\Lambda})}$ has the phase shift characteristics shown in Figure 5.17.

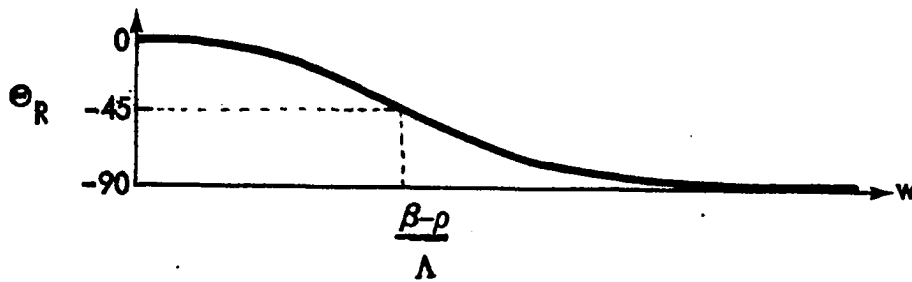


Figure 5.17. Reactor node phase shift

For the null frequency, the phase shift θ_R plus θ_p is equal to -90° , where θ_p is the phase angle due to the time delay function, p . If something is done to the system to increase θ_p (in a negative sense) the sink will occur at a lower frequency where θ_R is less and vice versa.

In the continuous model that is investigated in this thesis a space dependent coupling transfer function, K_{ij} , between two points, i and j , in the reactor can be defined in a similar manner to that defined for the two node system. In this case the time delay function, p_{ij} , and its phase angle, $\theta_{p_{ij}}$, will be space dependent and also will be dependent on the nuclear parameter of the coupling region through which the perturbation propagate from one core to the other.

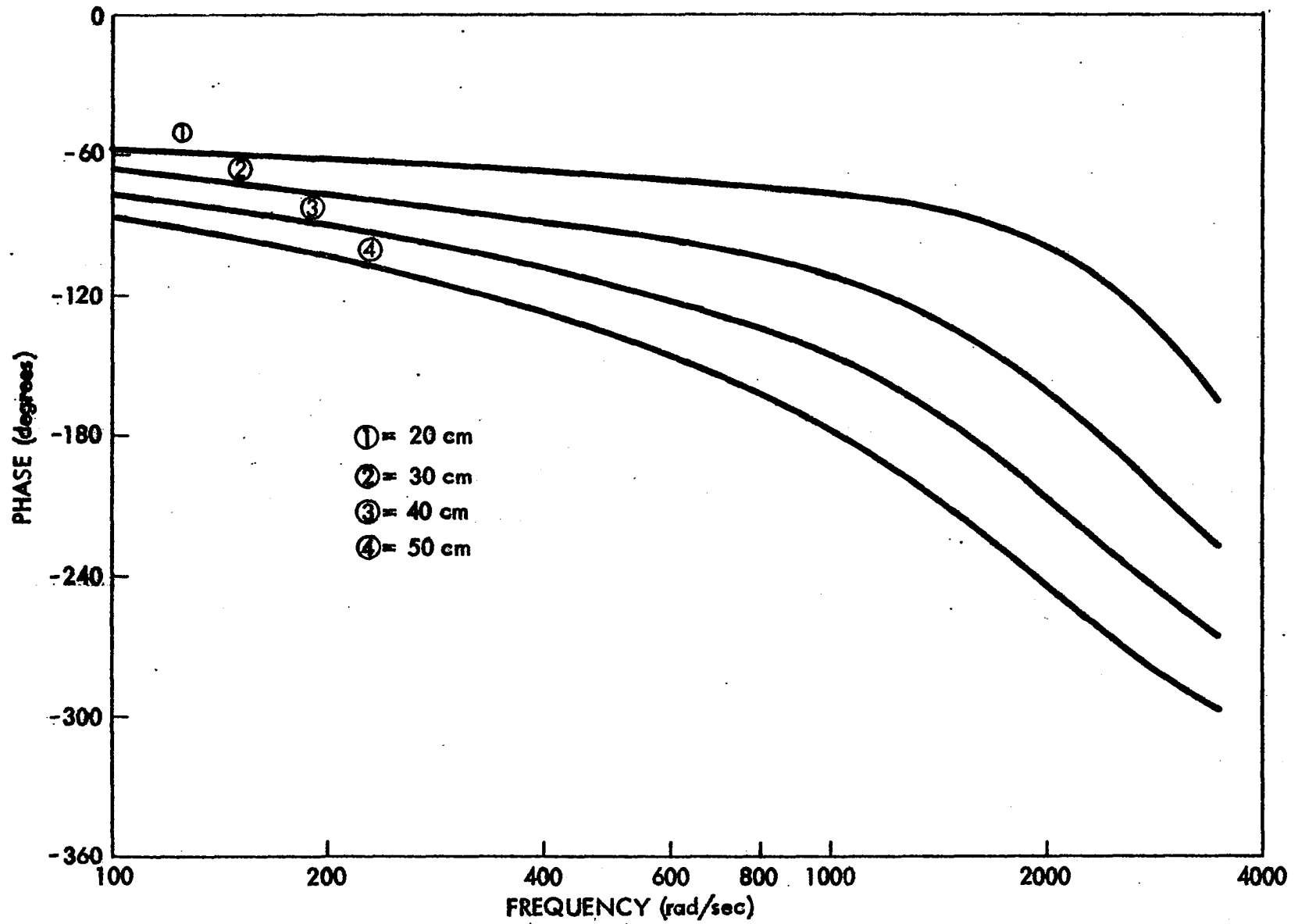
Since the space-dependent noise model used in this thesis is rather involved it is difficult to develop a quantitative explanation for the behavior shown in these results. In the

interest of exploring these results in more depth it was decided to use the sensitivity, as suggested by Equation 5.2, of the sink frequency to the time delay function as a means of developing an explanation of the sink frequency behavior.

For the two-node model, the phase shift of the time delay function is the important parameter in determining the sink frequency. Thus it would seem desirable to develop a model that gives the phase shift across the coupling region. If it can be shown how the phase shift behaves with coupling region parameters it could predict the trend shown by the sink behavior as shown in Figures 5.5, 5.13 and 5.14. For this analysis the time delay function was assumed to be described by the neutron wave theory.

A study of the phase shift shown by the neutron wave and its dependence on removal cross section, distance, and absorption cross section is developed in the Appendix. This wave model is applied to an infinite non-multiplying system, using two group diffusion theory with arbitrary source strengths. Of course some discrepancy should be expected between the wave model and the original models that are investigated since one system is infinite and the other is finite, also the wave model is nonmultiplying while the original systems are multiplying ones. Figure 5.18 shows the phase angle of the thermal neutron wave with distance as a parameter. According to this figure the phase angle of the

Figure 5.18. Phase angle of thermal neutron wave with distance as a parameter



neutron wave increases with distance which means that increasing distance increases the phase shift of the time delay function and cause the sink to shift to a lower frequency which is in agreement with the results shown on Figures 5.5 and 5.7. The wave model predicts that the second sink, as a function of spacing, would not behave in an opposite trend to that of the first sink.

Figure 5.19 shows that the phase shift of the neutron wave increases at low frequency and decreases at high frequency with increasing removal cross section which is in agreement with the results shown in Figure 5.13. It is shown that the first sink decreases with increasing removal cross section, which means that θ_p increases, and the second sink increases with increasing removal cross section which means that θ_p decreases at this second sink. However it was found that this wave model failed to explain the behavior of the sink with absorption cross section. Figure 5.20 shows the phase angle of the neutron wave as a function of absorption cross section. However it is shown in Figure 5.20 that at high frequency the phase angle is almost independent of the absorption cross section which is in agreement with the results shown in Figure 5.14. It can be observed that the sink frequency is almost insensitive to the absorption cross section at high cross sections.

It is found that the magnitude of the wave increases with

Figure 5.19. Phase angle of thermal neutron wave with removal cross section as a parameter

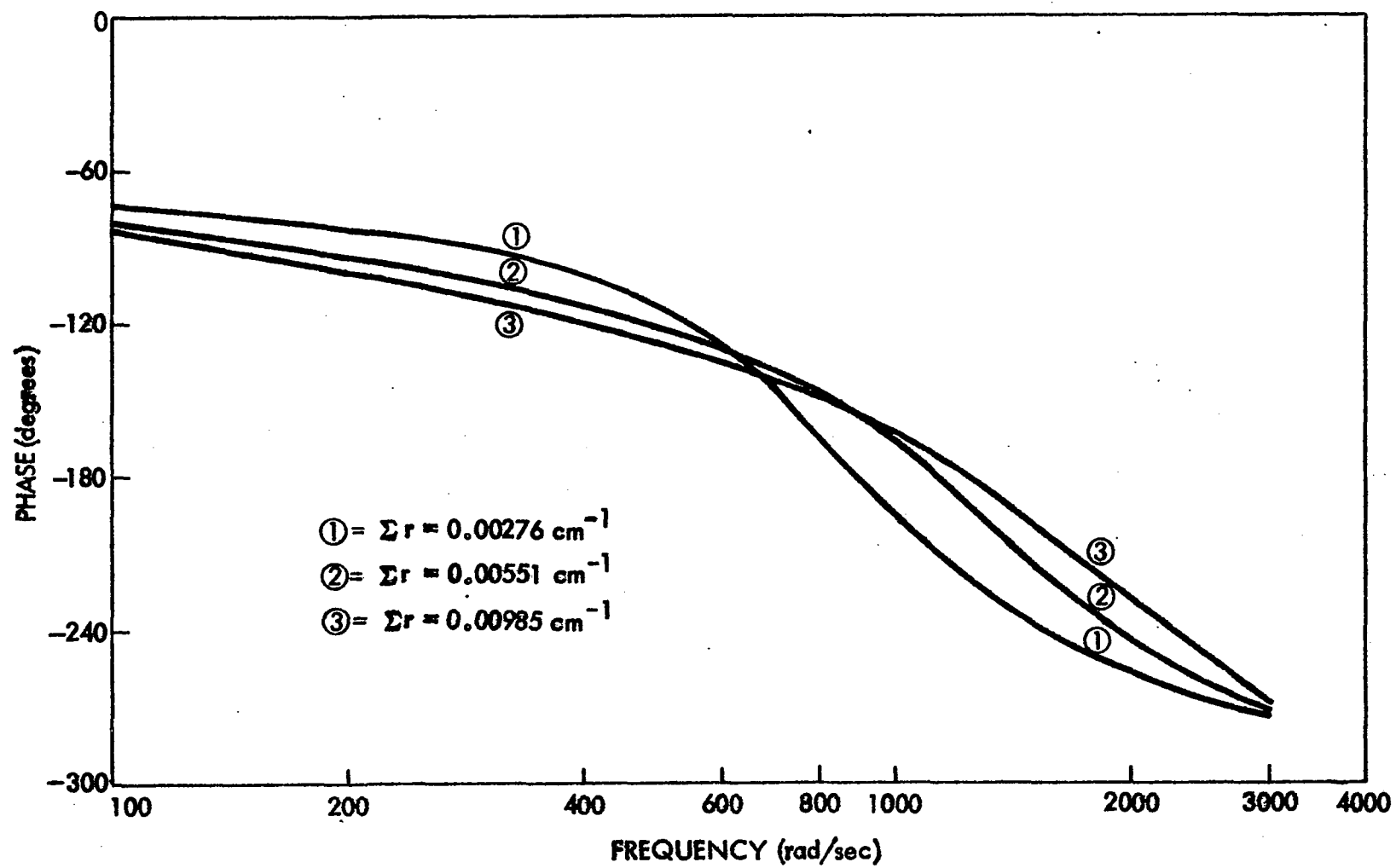
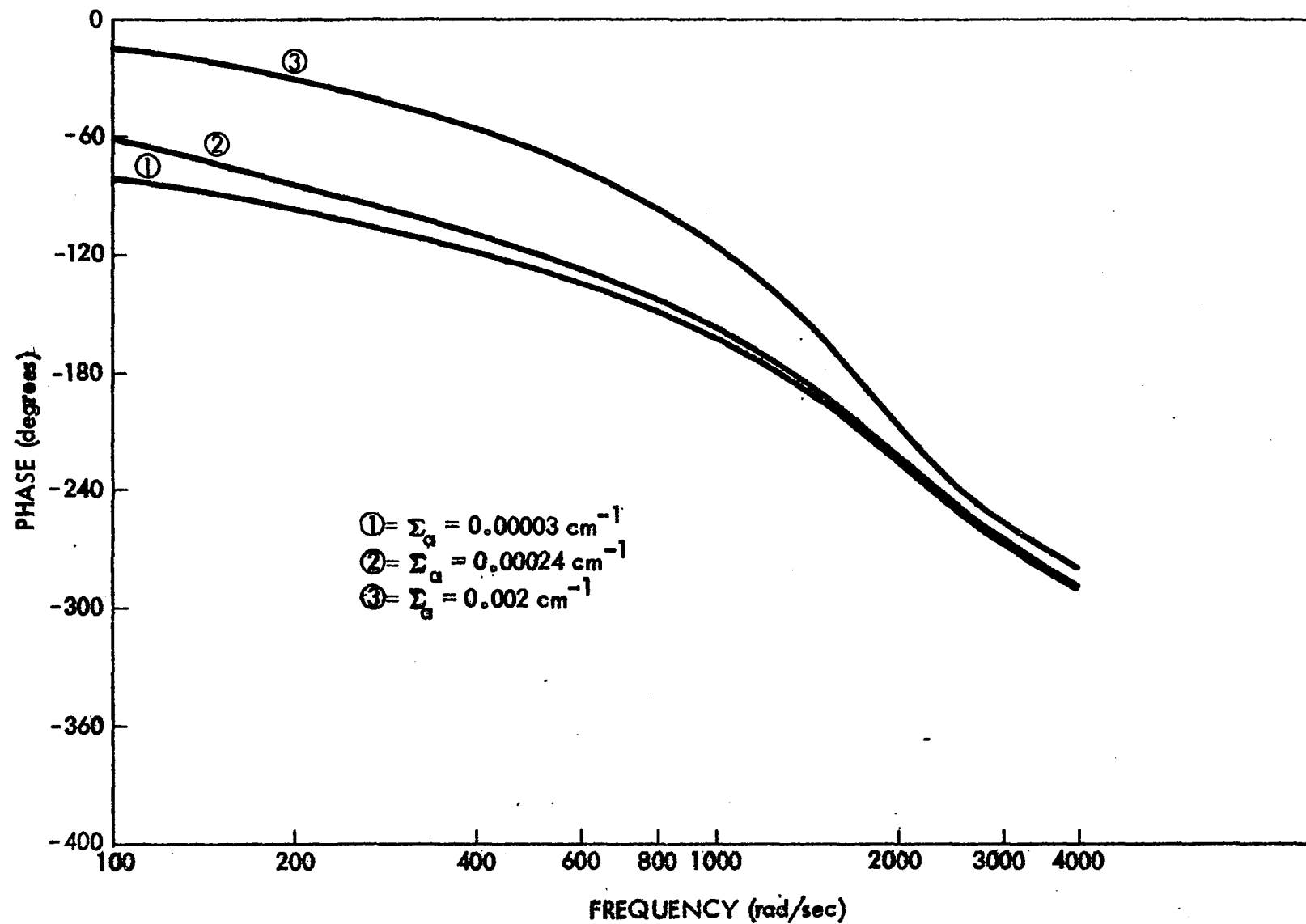


Figure 5.20. Phase angle of thermal neutron wave with absorption cross section as a parameter



removal cross section as expected since increasing the removal cross section increases the value of the thermal flux.

Also, it was found that the magnitude of the neutron wave decreased with increased distance and with increased absorption cross section. This is reasonable since increasing either of these should attenuate the wave magnitude.

VI. CONCLUSIONS

Within the scope of this investigation the following conclusions are justified.

1. For symmetric cases the CSDF is real and the sink frequency, if it exists, happens when the function crosses the zero of the real axis. For nonsymmetric cases the CSDF is complex and the sink frequency, if it exists, happens at a phase shift of -180° or -270° and the real part goes to zero.
2. The existence of a sink and the frequency at which it takes place is very sensitive to coupling region size and its nuclear parameters. For example no sinks were found for 1-4 and 1-5 CSDF in case of 25 cm graphite coupling region. On the other hand the 25 cm heavy water coupling region results showed distinctive sinks for the 1-4 and 1-5 CSDF. It is to be noted that the second sink has much less sensitivity to spacing than the first sink.
3. Changing the removal cross section affects the two sinks significantly. Increasing the removal cross section decreases the first sink frequency and increases the second sink frequency.
4. The sink frequency decreases with increasing absorption

cross section but the rate of decrease is high at low values of cross section and is very small at high values.

5. The neutron wave model has been shown to be a satisfactory model for explaining the sink behavior as a function of spacing and removal cross section. However there are discrepancies between the wave model phase shift and the sink frequency behavior when the thermal neutron absorption cross section is used as a parameter.

VII. SUGGESTIONS FOR FURTHER WORK

The following topics are suggested as areas for future work in which a contribution in the area investigated here could be made.

1. Measure the sink frequency as a function of coupling material and its thickness experimentally to provide a check for the analytic results shown in this work.
2. Study the effect of changing the diffusion coefficients of the neutron groups on the sink frequency and a check by the wave model.
3. Develop a wave model for a finite-multiplying system.
4. Develop a CSDF between fast neutron groups and between fast and slow groups.
5. Investigate the sink frequency as a function of enrichment of the fuel regions.

VIII. LITERATURE CITED

1. Akcasu, Z. A. and Osborn, R. K. Application of Langevin's technique to space and energy - Dependent noise analysis. Nuc. Sci. and Eng. 26: 13-25. 1966.
2. Albrecht, R. W. and Seifritz, W. The coherence function: A measure of spatially dependent nuclear reactor parameters. U.S./Japan Seminar on Reactor Noise Analysis. Tokyo, Japan, September 2-7, 1968. Seattle, Washington, Department of Nuclear Engineering, University of Washington. 1968.
3. Albrecht, R. W. and Seifritz, W. Fundamental properties of the coherence function in symmetrical two-node systems. Nukleonik 11: 143-148. 1968.
4. Balcomb, J. D., Demuth, M. B. and Gyftopoulos, E. P. A cross correlation method for measuring the impulse response of reactor systems. Nuc. Sci. and Eng. 11: 159-166. 1961.
5. Betancourt, J. M. Analysis of coupled core reactors using the natural mode approximation. Unpublished Ph.D. thesis. Ames, Iowa, Library, Iowa State University. 1966.
6. Carter, N. Solution of space-time kinetic equations for coupled-core nuclear reactors. Unpublished Ph.D. thesis. Ames, Iowa, Library, Iowa State University. 1967.
7. Carter, N. and Danofsky, R. The application of the calculus of variations and the method of Green's function to the solution of coupled core kinetics equations. In Chezem, G. G. and Kohler, W. H., editors. Conference on Coupled Reactor Kinetics. College Station, Texas, January, 1967. Pp. 749-769. College Station, Texas, The Texas A and M Press. 1967.
8. Danofsky, R. A. A space-dependent reactor-noise formulation utilizing modal expansions. Nuc. Sci. and Eng. 36: 28-38. 1969.
9. Dougherty, D. E. and Shen, C. N. The space-time neutron kinetic equations obtained by the semidirect variational method. Nuc. Sci. and Eng. 13: 141-148. 1962.

10. Foderaro, A. and Garabedian, M. L. A new method for the solution of group diffusion equations. Nuc. Sci. and Eng. 8: 44-52. 1960.
11. Foderaro, A. and Garabedian, M. L. Two group reactor kinetics. Nuc. Sci. and Eng. 14: 22-29.
12. Gyftopoulos, E. P. Some applications of mathematical methods to nuclear engineering at the Massachusetts Institute of Technology. Atomic Energy Commission Symposium Series 7: 1-27. 1966.
13. Hendrickson, R. A. Cross-spectral density measurements in a coupled-core reactor. Unpublished Ph.D. thesis. Ames, Iowa, Library, Iowa State University. 1966.
14. Kaplan, S. Modal analysis. In Radkousky, A., editor. Naval reactor physics handbook. Vol. 1. Pp. 966-977. Washington, D.C., U.S. Government Printing Office. 1964.
15. Kaplan, S. The property of finality and the analysis of problems in reactor space-time kinetics by various modal expansions. Nuc. Sci. and Eng. 9: 357-361. 1961.
16. Kaplan, S., Henry, A. F., Margolls, S. D. and Taylor, J. J. Space time reactor dynamics. United Nations International Conference on the Peaceful Uses of Atomic Energy 3: 41. 1964.
17. Lamarsh, J. R. Introduction to nuclear reactor theory. Reading, Massachusetts, Addison-Wesley Publishing Co., Inc. 1966.
18. Lennox, D. H., Spinrand, B. I., Kelber, C. N., Armstrong, R. H. and Kolb, W. L. The argonaut reactor: A generalized reactor facility for nuclear technology training and research. United Nations International Conference on Peaceful Uses of Atomic Energy 2: 265. 1958.
19. Merritt, I. W. Spatially dependent frequency response of coupled core reactors. Unpublished Ph.D. thesis. Ames, Iowa, Library, Iowa State University. 1968.

20. Moore, M. N. The determination of reactor transfer function from measurements at steady operation. Nuc. Sci. and Eng. 3: 387-394. 1958.
21. Moore, M. N. Noise field of a reactor. Atomic Energy Commission Symposium Series 4: 13-27. 1964.
22. Natelson, M., Osborn, R. K. and Shure, F. Space and energy effects in reactor fluctuation experiments. J. Nuc. Energy 20, Parts A/B: 557-585. 1966.
23. Nodean, W. C. The response of a coupled core reactor to a localized oscillation of the absorption cross section. Unpublished Ph.D. thesis. Ames, Iowa, Library, Iowa State University. 1969.
24. Osborn, R. K. and Natelson, N. M. Kinetic equations for neutron distributions. J. Nucl Energy 19, Parts A/B: 619-639. 1965.
25. Rajagopal, V. Determination of reactor transfer functions by statistical correlation methods. Nuc. Sci. and Eng. 12: 218-224. 1962.
26. Ricker, C. W., Hanauer, S. H. and Mann, E. R. Measurement of reactor fluctuation spectra and sub-critical reactivity. U.S. Atomic Energy Commission Report ORNL-TM-1066 (Oak Ridge National Lab., Tenn.) 1965.
27. Seifritz, W. and Albrecht, R. W. Measurement and analysis of the coupled core coherence function in a two node symmetrical reactor. Nukleonik 11: 149-154. 1968.
28. Seifritz, W., Stegemann, D., and Vöth, W. Two detector cross-correlation experiments in the fast-thermal argonaut reactor. U.S. Atomic Energy Commission Symposium Series 9: 195-216. 1966.
29. Sheff, J. R. and Albrecht, R. W. The space dependence of reactor noise. I. Theory. Nuc. Sci. and Eng. 24: 246-259. 1966.
30. Sheff, J. R. and Albrecht, R. W. The space dependence of reactor noise. II. Calculations. Nuc. Sci. and Eng. 26: 207-221.

31. Weinberg, A. M. and Schweinler, H. C. Theory of oscillating absorber in a chain reactor. Physical Review 74: 851-863. 1948.

IX. ACKNOWLEDGMENTS

I wish to thank Dr. Richard Danofsky, and Dr. Glenn Murphy for their assistance and interest during the preparation of this work. I also gratefully acknowledge support by the Egyptian Government and the Institute of International Education by the award of a fellowship to study nuclear engineering and acknowledge the many helpful discussions and suggestions made by Dr. Danofsky during the course of this work.

I wish to acknowledge my parents who have been most encouraging and helpful through my education.

I also want to thank Dr. Glenn Murphy for his guidance through my graduate study.

X. APPENDIX

In this section the magnitude and phase angle of thermal neutron wave are developed as follows.

Consider an infinite planar source which emits slow and fast neutrons and oscillates, in both, sinusoidally with frequency ω into an infinite homogeneous medium. Since the source plane and the medium are both infinite, the flux at any point in the medium can be a function only of the distance from the plane. One can write the time dependent two groups diffusion equation as follows.

$$D_F \nabla^2 \phi_F(x,t) - \Sigma_r \phi_F(x,t) = \frac{1}{v_F} \frac{\partial \phi_F(x,t)}{\partial t} \quad (10.1)$$

$$D_S \nabla^2 \phi_S(x,t) - \Sigma_a \phi_S(x,t) + \Sigma_r \phi_F(x,t) = \frac{1}{v_S} \frac{\partial \phi_S(x,t)}{\partial t} \quad (10.2)$$

where

D_F = fast diffusion coefficient

D_S = slow diffusion coefficient

ϕ_F = fast flux

ϕ_S = slow flux

Σ_r = removal cross section

Σ_a = thermal absorption cross section

v_F = fast neutron velocity

v_S = slow neutron velocity

the fast source, $S_F(x,t)$, can be written as

$$S_F(x,t) = S_F(0) + \Delta S_F(x) e^{j\omega t}$$

and the slow source, $S_S(x,t)$, can be written as

$$S_S(x,t) = S_S(0) + \Delta S_S(x) e^{j\omega t} \quad (10.3)$$

where $S(0)$ is a steady state source magnitude and $\Delta S(x)$ represents the magnitude of the oscillating part. Since there are no sources present in the medium itself, $S(0)$ and $\Delta S(x)$ are zero every where in the medium except at $x=0$.

Since the diffusion equation is linear one can represent the flux response as

$$\phi_F(x,t) = \phi_F(0) + \psi_F(x) e^{j\omega t} \quad (10.4)$$

and

$$\phi_S(x,t) = \phi_S(0) + \psi_S(x) e^{j\omega t} \quad (10.5)$$

Where $\phi_F(0)$ and $\phi_S(0)$ the flux due to a steady condition in the medium. Substituting Equation (10.4) and (10.5) in Equations (10.1) and (10.2) and eliminating the steady state terms one gets

$$D_F \frac{d^2 \psi_F}{dx^2} - \Sigma_r \psi_F - \frac{j\omega}{v_F} \psi_F = 0 \quad (10.6)$$

and

$$D_S \frac{d^2 \psi_S}{dx^2} - \Sigma_a \psi_S - \frac{j\omega}{v_S} \psi_S + \Sigma_r \psi_F = 0 \quad (10.7)$$

Let

$$\left(\frac{\Sigma_r}{D_F} + \frac{j\omega}{D_F v_F} \right) = \beta_F$$

and

$$\left(\frac{\Sigma_a}{D_S} + \frac{j\omega}{v_S D_S} \right) = \beta_S$$

Let

$$U_F = (\beta_F)^{\frac{1}{2}}$$

$$U_S = (\beta_S)^{\frac{1}{2}}$$

Then

$$\frac{d^2 \psi_F}{dx^2} - \beta_F \psi_F = 0 \quad (10.8)$$

$$\frac{d^2 \psi_S}{dx^2} - \beta_S \psi_S + \frac{\Sigma_r}{D_S} \psi_F = 0 \quad (10.9)$$

The solution of (10.8) is

$$\psi_F = A_1 e^{-U_F x} + A_2 e^{U_F x} \quad (10.10)$$

Considering positive values of x , it is evident that A_2 must be taken equal to zero; otherwise the flux would become infinite with increasing x . Then

$$\psi_F = A_1 e^{-U_F x} \quad (10.11)$$

A_1 can be found from the source condition

$$\begin{aligned} \lim_{x \rightarrow 0} J(x) &= -\lim_{x \rightarrow 0} D_F \frac{d\psi_F}{dx} = D_F U_F A_1 e^{-U_F x} = U_F D_F A_1 \\ &= \frac{\Delta S_F(0)}{2} = SF \end{aligned}$$

then

$$A_1 = \frac{SF}{D_F U_F}$$

and

$$\psi_F = \frac{SF e^{-U_F x}}{D_F U_F}$$

one can write

$$U_F = \text{REF} + j \text{ImF}$$

and

$$U_S = \text{RES} + j \text{ImS}$$

$$\psi_F = \frac{SF(\text{REF} - j \text{ImF}) e^{-U_F x}}{D_F [(\text{REF})^2 + (\text{ImF})^2]} \quad (10.12)$$

Equation (10.9) is a nonhomogenous linear differential equation with $\sum_r \frac{x}{D_S} \psi_F$ as the nonhomogeneous part. The complete solution, ψ_S , can be written as the summation of a homogeneous, ψ_{sH} , and particular, ψ_{sp} , solutions. The homogeneous part of Equation (10.9) has the form

$$\frac{d^2 \psi_{sH}}{dx^2} - \beta_S \psi_{sH} = 0 \quad (10.13)$$

The solution of (10.13) is

$$\psi_{sH} = C_1 e^{-U_s x} + C_2 e^{U_s x} \quad (10.14)$$

Following the same argument which led to Equation (10.11) Equation (10.14) can be written as

$$\psi_{sH} = C_1 e^{-U_s x} \quad (10.15)$$

To get the particular solution, the solution

$$\psi_{sp} = M e^{-U_F x} \quad (10.16)$$

should be tried. Substituting this value of ψ_{sp} in Equation (10.9) it follows that

$$MU_F^2 e^{-U_F x} - \beta_s M e^{-U_F x} = -\frac{\sum_r A_1}{D_s} e^{-U_F x} \quad (10.17)$$

and

$$MU_F^2 - \beta_s M = M\beta_F - \beta_s M = -\frac{\sum_r A_1}{D_s}$$

then

$$M = -\frac{\sum_r A_1}{D_s(\beta_F - \beta_s)}$$

and

$$\begin{aligned} \psi_s &= \psi_{sH} + \psi_{sp} \\ &= C_1 e^{-U_s x} - \frac{\sum_r A_1 e^{-U_F x}}{D_s(\beta_F - \beta_s)} \end{aligned} \quad (10.18)$$

$$= C_1 e^{-U_S x} - \frac{\Sigma_r \cdot SF(REF - j \text{Im}F) e^{-U_F x}}{D_F \cdot D_S (\beta_F - \beta_S) [(REF)^2 + (\text{Im}F)^2]}$$

To find C_1 , apply the source condition

$$-\lim_{x \rightarrow 0} D_S \frac{d\psi_S}{dx} = \frac{\Delta S_S(0)}{2} = SS$$

Then

$$D_S C_1 U_S - \frac{\Sigma_r \cdot SF \cdot (REF - j \text{Im}F) U_F}{D_F (\beta_F - \beta_S) [(REF)^2 + (\text{Im}F)^2]} = SS \quad (10.19)$$

and

$$\begin{aligned} C_1 &= \frac{SS}{D_S \cdot U_S} + \frac{\Sigma_r \cdot SF(REF - j \text{Im}F) U_F}{D_S \cdot U_S \cdot D_F \cdot (\beta_F - \beta_S) [(REF)^2 + (\text{Im}F)^2]} \quad (10.20) \\ &= \frac{SS \cdot (RES - j \text{Im}S)}{D_S [(RES)^2 + (\text{Im}S)^2]} + \frac{\Sigma_r \cdot SF(RES - j \text{Im}S)}{D_F \cdot D_S (\beta_F - \beta_S) [(RES)^2 + (\text{Im}S)^2]} \end{aligned}$$

Since β_F and β_S are complex it can be shown that

$$\begin{aligned} \frac{1}{(\beta_F - \beta_S)} &= \frac{\left(\frac{\Sigma_r}{D_F} - \frac{\Sigma_s}{D_S}\right) - j\left(\frac{\omega}{v_F D_F} - \frac{\omega}{v_S D_S}\right)}{\left(\frac{\Sigma_r}{D_F} - \frac{\Sigma_a}{D_S}\right)^2 + \left(\frac{\omega}{v_F D_F} - \frac{\omega}{v_S D_S}\right)^2} \\ &= \frac{\alpha - j\Delta}{\alpha^2 + \Delta^2} \quad (10.21) \end{aligned}$$

C_1 can be written as

$$C_1 = \frac{SS \cdot (RES - j \text{ImS})}{D_S [(RES)^2 + (\text{ImS})^2]} + \frac{\Sigma_r \cdot SF \cdot (RES - j \text{ImS}) (\alpha - j\Delta)}{D_F \cdot D_S (\alpha^2 + \Delta^2) [(RES)^2 + (\text{ImS})^2]}$$

$$= \frac{SS \cdot (RES - j \text{ImS})}{D_S [(RES)^2 + (\text{ImS})^2]} + \frac{\Sigma_r \cdot SF [\alpha \cdot RES - \Delta \cdot \text{ImS}] - j [\Delta \cdot RES + \alpha \cdot \text{ImS}]}{D_F D_S (\alpha^2 + \Delta^2) [(RES)^2 + (\text{ImS})^2]}$$

(10.22)

Let

$$Y_S = [(RES)^2 + (\text{ImS})^2]$$

and

$$Y_F = [(REF)^2 + (\text{ImF})^2]$$

then

$$C_1 = \left[\frac{SS \cdot RES}{D_S Y_S} + \frac{\Sigma_r \cdot SF \cdot (\alpha \cdot RES - \Delta \cdot \text{ImS})}{D_F D_S (\alpha^2 + \Delta^2) Y_S} \right]$$

$$- j \left[\frac{SS \cdot \text{ImS}}{D_S Y_S} + \frac{\Sigma_r \cdot SF \cdot (\Delta \cdot RES + \alpha \cdot \text{ImS})}{D_F D_S (\alpha^2 + \Delta^2) Y_S} \right]$$

$$= REC - j \text{ImC} \quad (10.23)$$

The slow flux can then be written as

$$\psi_S = (REC - j \text{ImC}) e^{-U_S x} + \frac{\Sigma_r \cdot SF (\alpha - j\Delta) (REF - j \text{ImF}) e^{-U_F x}}{D_F \cdot D_S \cdot (\alpha^2 + \Delta^2) [(REF)^2 + (\text{ImF})^2]}$$

$$= [(REC)^2 + (\text{ImC})^2]^{\frac{1}{2}} \cdot e^{-j \tan^{-1} \left(\frac{\text{ImC}}{REC} \right)} \cdot e^{-RES \cdot x} \cdot e^{-j \text{ImS} \cdot x}$$

$$\begin{aligned}
& + \frac{\Sigma_r \cdot SF \cdot e^{-U_F x} \cdot e^{-j \tan^{-1}(\frac{\Delta}{\alpha})} \cdot e^{-j \tan^{-1}(\frac{ImF}{REF})}}{D_F \cdot D_S \cdot (\alpha^2 + \Delta^2)^{\frac{1}{2}} \cdot Y_F^{\frac{1}{2}}} \\
& = [(REC)^2 + (ImC)^2]^{\frac{1}{2}} e^{-RES \cdot x} [\cos(ImS \cdot x + \tan^{-1} \frac{ImC}{REC}) \\
& \quad - j \sin(ImS \cdot x + \tan^{-1} \frac{ImC}{REC})] \\
& + \frac{\Sigma_r \cdot SF \cdot e^{-REF \cdot x} [\cos(ImF \cdot x + \tan^{-1} \frac{\Delta}{\alpha} + \tan^{-1} \frac{ImF}{REF}) }{D_F \cdot D_S \cdot (\alpha^2 + \Delta^2)^{\frac{1}{2}} \cdot [(REF)^2 + (ImF)^2]^{\frac{1}{2}}} \quad (10.24)
\end{aligned}$$

Let

$$\theta_S = ImS \cdot x + \tan^{-1} \frac{ImC}{REC} ,$$

$$\theta_F = ImF \cdot x + \tan^{-1} \frac{\Delta}{\alpha} + \tan^{-1} \frac{ImF}{REF} ,$$

$$\Lambda_S = [(REC)^2 + (ImC)^2]^{\frac{1}{2}} e^{-RES \cdot x}$$

and

$$\Lambda_F = \frac{\Sigma_r \cdot SF \cdot e^{-REF \cdot x}}{D_F \cdot D_S \cdot (\alpha^2 + \Delta^2)^{\frac{1}{2}} \cdot [(REF)^2 + (ImF)^2]^{\frac{1}{2}}}$$

Then

$$\begin{aligned}
\psi_S &= \Lambda_S [\cos \theta_S - j \sin \theta_S] + \Lambda_F [\cos \theta_F - j \sin \theta_F] \\
&= \Lambda_S \cos \theta_S + \Lambda_F \cos \theta_F - j [\Lambda_S \sin \theta_S + \Lambda_F \sin \theta_F] \\
&= RE - j Im \quad (10.25)
\end{aligned}$$

The phase angle of the thermal wave can be written as

$$\theta_T = \tan^{-1} \left(\frac{-\text{Im}}{\text{RE}} \right) \quad (10.26)$$

and the magnitude of the wave is

$$\text{Mag} = [(\text{RE})^2 + (\text{Im})^2]^{\frac{1}{2}} \quad (10.27)$$

A computer program is written for evaluating Equations (10.22) and (10.23) for different Σ_r , x and Σ_a . The results are discussed in section 5.